LAGRANGE GAGE STUDIES OF NONIDEAL EXPLOSIVES CONTAINING NH_4NO_3

Final Report

June 1983

By: M. Cowperthwaite and J. T. Rosenberg

Prepared for:

U. S. ARMY RESEARCH OFFICE
P.O. Box 12211
Research Triangle Park, NC 27709

Contract No. DAAG29-80-C-0076

SRI Project PYU 1290

SRI International
333 Ravenswood Avenue
Menlo Park, California 94025
(415) 326-6200
TWX: 910-373-2046
Telex: 334 486

UNCLASSIFIED

SECURITY CLASSIFICATION OF THIS PAGE (When Data Entered)

REPORT DOCUMENTATION PAGE		READ INSTRUCTIONS BEFORE COMPLETING FORM
1. REPORT NUMBER	2. GOVT ACCESSION NO.	3. RECIPIENT'S CATALOG NUMBER
4. TITLE (and Subtitle) LAGRANGE GAGE STUDIES OF NONIDEAL EXPLOSIVES CONTAINING NH_4NO_3		5. TYPE OF REPORT & PERIOD COVERED Final Report 6. PERFORMING ORG. REPORT NUMBER PYU-1290
7. AUTHOR(s) M. Cowperthwaite and J. T. Rosenberg		8. CONTRACT OR GRANT NUMBER(s) DAAG29-80-0076
9. PERFORMING ORGANIZATION NAME AND ADDRESS SRI International 333 Ravenswood Avenue Menlo Park, CA 94025		10. PROGRAM ELEMENT PROJECT, TASK AREA & WORK UNIT NUMBERS
11. CONTROLLING OFFICE NAME AND ADDRESS U.S. Army Research Office P.O. Box 12211 Research Triangle Park, NC 27709		12. REPORT DATE June 1983 13. NUMBER OF PAGES 70
14. MONITORING AGENCY NAME & ADDRESS(if different from Controlling Office)		15. SECURITY CLASS (of this report) Unclassified 15a. DECLASSIFICATION DOWNGRADING SCHEDULE

16. DISTRIBUTION STATEMENT (of this Report)

Approved for public release; distribution unlimited.

17. DISTRIBUTION STATEMENT (of the abstract entered in Block 20, if different from Report)

18. SUPPLEMENTARY NOTES

The view, opinions, and/or findings contained in this report are those of the authors and should not be construed as an official Department of the Army position, policy, or decision unless so designated by other documentation.

19. KEY WORDS (Continue on reverse side if necessary and identify by block number)

Ideal detonation	Particle velocity gages	Unattainment of chemical equilibrium
Nonideal detonation	Lagrange analysis	Reaction times
Hugoniot curve	Amatex 20	NH_4NO_3
Chapman-Jouguet state	Detonation parameters	
Embedded Lagrange gages	Incomplete decomposition	

20. ABSTRACT (Continue on reverse side if necessary and identify by block number)

Theoretical and experimental studies of planar detonation waves in Amatex 20 were performed to obtain a better understanding of the role of NH_4NO_3 (AN) in the detonation process in explosives formulated from RDX, TNT, and AN.

The theoretical work was performed to provide a more definitive and realistic treatment of steady-state detonation waves in such composite explosives. The treatment developed for such waves extends the classical

DD FORM 1 JAN 73 1473 EDITION OF 1 NOV 65 IS OBSOLETE

UNCLASSIFIED

SECURITY CLASSIFICATION OF THIS PAGE (When Data Entered)

20. ABSTRACT (continued)

Zelodovich-von Neumann-Doering (ZND) model for ideal detonation into a prototype model for nonideal detonation. The kinetic processes responsible for nonideal behavior were assumed to be incomplete decomposition of the slowest reacting explosive component, and the incomplete attainment of chemical equilibrium among the detonation products from the different explosive components. The constitutive relationship for the shocked reacting explosive was constructed with different equations of state for the explosives and their products and enough reaction coordinates to account for this type of nonideality. This constitutive relationship was combined with the Rankine-Hugoniot (RH) relationships, and the Chapman-Jouguet (CJ) sonic condition to derive equations for (1) the CJ parameters in and the propagation velocity of a steady-state nonideal detonation wave, and (2) the particle velocity in terms of the reaction coordinates in a steady-state nonideal detonation wave. Detonation parameters and Lagrange particle velocity histories were calculated for nonideal detonation waves in an explosive modeling Amatex 20.

The experimental work was performed to obtain a more complete characterization of the detonation process in Amatex 20. The mean particle size of AN in the Amatex 20 charges was increased from the baseline value of ~0.7 mm to a value of ~2 mm. Multiple Lagrange particle velocity gage experiments were performed and analyzed to obtain a quantitative description of planar detonation in this coarse-grained Amatex 20. The experimentally determined CJ parameters for this coarse-grained Amatex 20 (D = 6.85 mm/μs, u_{CJ} = 1.67 mm/μs, p_{CJ} = 182 kbar, v_{CJ} = 0.4742 cm^3/g, K_{CJ} = 3.10, τ_{CJ} ~ 0.63 μs) and those determined for the baseline Amatex 20 (D = 6.95 mm/μs, u_{CJ} = 1.94 mm/μs, p_{CJ} = 217 kbar, v_{CJ} = 0.4470 cm^3/g, K_{CJ} = 2.58, τ_{CJ} ~ 0.5 μs) clearly demonstrate that the particle size of AN influences the detonation process in Amatex 20. Kamlet's semi-empirical method for calculating detonation parameters was modified and used to interpret the differences between these sets of CJ parameters. Application of this method led us to formulate the following hypotheses about the nonideal planar detonation process in Amatex 20: (1) AN with a mean particle size of 0.7 mm decomposes completely in the reaction zone, but the decomposition products of RDX, TNT, and AN do not attain chemical equilibrium, and (2) AN with a mean particle size of ~2 mm does not decompose completely in the reaction zone, and the detonation products of RDX, TNT, and AN do not attain chemical equilibrium.

ACKNOWLEDGMENTS

We gratefully acknowledge many valuable contributions that were made to this work by our colleagues and coworkers. We are especially indebted to A. P. Torres and J. Sanchez of Los Alamos National Scientific Laboratory for their cooperation and proficiency in casting the targets used to perform the detonation experiments. At SRI, we particularly acknowledge and thank F. B. Galimba for constructing the gage blocks, D. F. Walter and H. E. Hanna for assistance with electronic and site instrumentation in performing the experiments, and B. Y. Lew, J. Kempf, and Y. D. Murray for digitizing the particle velocity records and performing Lagrange analyses.

We also acknowledge discussions on detonation calculations with Dr. J. M. Short and Dr. M. J. Kamlet of Naval Surface Weapons Center, White Oak Laboratory, Silver Spring.

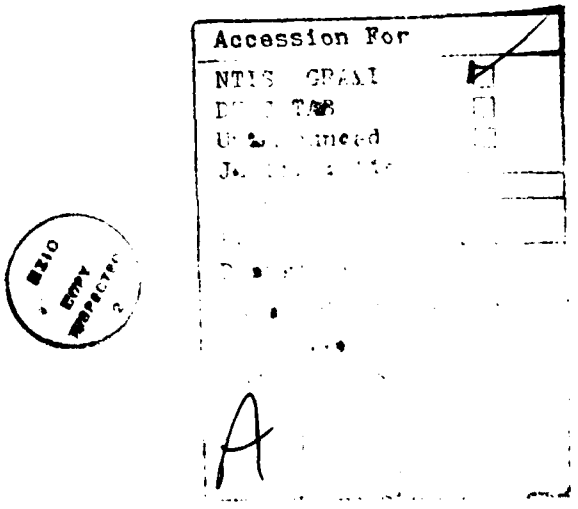

CONTENTS

ACKNOWLEDGMENTS iii

LIST OF FIGURES vii

LIST OF TABLES ix

I INTRODUCTION 1

II THEORETICAL STUDY 3

Governing Equations 4

Flow Equations 4
Equations for the Explosive 6
Constitutive Relationship for Reacting Composite Explosive 9

Nonideal Steady-State Detonation Waves 13

Chapman-Jouguet Conditions 13
Dependence of Particle Velocity on Reaction Coordinates 17

Model Nonideal Detonation Calculations 20

Detonation Parameters 20
Lagrange Particle Velocity Histories 24

Conclusions 33

III EXPERIMENTS 35

Basic Technique 35

EPV Gages 35

Basic Operation 35
Emplacement 39

Targets 39

Coarse-Grained Amatex 20 39
Target Configuration 39

Data 43

Lagrange Analysis 45

Procedure 45
Selection and Smoothing of Particle Velocity Histories 46
Results 48

Discussion 48

The Detonation Process in Coarse-Grained Amatex 20 48

The Role of AN in the Detonation Process in Amatex 20 53

REFERENCES 59

FIGURES

1a	Particle Velocity Versus Time in Reaction Zone Calculated with $n_1 = 3$, $f = 4$, and $n_2 = 2$	27
1b	Reaction Coordinates Versus Particle Velocity in Reaction Zone Calculated with $n_1 = 3$, $f = 4$, and $n_2 = 2$	28
2a	Particle Velocity Versus Time in Reaction Zone Calculated with $n_1 = 2$, $f = 3$, and $n_2 = 2$	29
2b	Reaction Coordinates Versus Particle Velocity in Reaction Zone Calculated with $n_1 = 2$, $f = 3$, and $n_2 = 2$	30
3a	Particle Velocity Versus Time in Reaction Zone Calculated with $n_1 = 3$, $f = 3$, and $n_2 = 3$	31
3b	Reaction Coordinates Versus Particle Velocity in Reaction Zone Calculated with $n_1 = 3$, $f = 3$, and $n_2 = 3$	32
4	Basic Configuration of Large-Scale Lagrange Particle Velocity Gage Experiments	36
5	Gage Block Used to Cast EPV Gages into Explosive Targets	38
6	Core Pattern for Coarse-Grained Amatex 20	40
7	Target Configuration and Dimensions	42
8	EPV Gage Records, Coarse-Grained Amatex 20, Shot 1290-2	44
9	Smoothed Particle Velocity Histories in Detonating Coarse-Grained Amatex 20, Shot 1290-2	49
10	Calculated Lagrange Pressure Histories at the Gage Positions in Detonating Coarse-Grained Amatex 20	50

11 Calculated Lagrange Pressure-Particle Velocity Shock Compression and Adiabatic Release Paths at the Gage Positions in Detonating Coarse-Grained Amatex 20 51

12 Calculated Lagrange Pressure-Specific Volume Shock Compression and Adiabatic Release Paths at the Gage Positions in Detonating Coarse-Grained Amatex 20 52

TABLES

1	Values of the Parameters for X_1, X_2, and X_3	21
2	Detonation Parameters for $\lambda_3 \leq 1$ and $\lambda_4 = 0.6\ \lambda_3$	23
3	Coarse-Grained Amatex 20 Composition and Density	41
4	Ammonium Nitrate Prill Particle Size, Coarse-Grained Amatex 20	41
5	Values of Detonation Parameters for RDX, TNT, AN and Amatex 20	56
6	Calculated CJ Parameters for Amatex 20	56

I INTRODUCTION

The overall objective of the research was to obtain a basic understanding of ammonium nitrate (AN) in the planar detonation process in composite military explosives formulated from RDX, TNT, and AN. Theoretical and experimental studies were performed to extend the previous work[1] performed under Contract No. DAAG29-76-C-0033.

The theoretical work was performed to provide a more definitive and realistic treatment of detonation in composite explosives such as Amatex 20. We addressed the general problem of detonation in a composite explosive X fabricated from three explosive components, X_1, X_2, and X_3. It is necessary in approaching this problem to identify and model rate processes that may influence the detonation process and give rise to nonideal behavior. The model for planar detonation in such composite explosives constructed in this report is based on the premise that certain chemical reactions do not proceed to completion in the steady-state reaction zone. In this case, nonideal behavior arises because not all the available chemical energy is used to support the propagation of the detonation wave.

The experimental work was performed to obtain a more complete characterization of the detonation process in Amatex 20. The mean particle size of the AN in the Amatex 20 charges was increased from the baseline value of about 0.7 mm to a value of about 2 mm. Multiple Lagrange particle velocity gage experiments were performed and analyzed to obtain a quantitative description of planar detonation in Amatex 20 containing this coarse-grained AN. Significant differences in the values of the detonation parameters in the charges containing base-line and coarse-grained AN clearly demonstrate that the detonation process in Amatex 20 is influenced by the particle size of the AN. The method developed by Kamlet[2-4] to calculate CJ parameters was modified[5] and used to interpret these differences.

II THEORETICAL STUDY

Our theoretical study is based on the assumption that planar one-dimensional detonation in our composite explosive can be treated as a Zeldovich-von Neumann-Doering[6-8] (ZND) wave. In this case, states in a steady-state detonation are governed by the Rankine-Hugoniot (RH) jump conditions[9] expressing the balance of mass, momentum, and energy in a steady-state flow. The flow becomes sonic at the Chapman-Jouguet (CJ) point where the global energy release rate (GERR) becomes zero, and when all the reactions contributing to the (GERR) are exothermic, the CJ point is at the end of the reaction zone. Exothermic reactions considered to contribute to the GERR are as follows:

- The global decompositions of the explosive components X_1, X_2, and X_3 into their detonation products in local chemical equilibrium.
- Reactions among the different detonation products of X_1, X_2, and X_3 as they mix and react to approach global chemical equilibrium.

We are now in a position to define "ideal" and "nonideal" detonation.

A steady-state ZND wave is said to be ideal when all the global decomposition reactions of the explosive components proceed to completion and the products of these reactions attain global chemical equilibrium. Otherwise it is said to be nonideal. This definition is compatible with the one we used previously[1] and leads us to assume that the two major factors responsible for nonideal behavior of our composite explosive are as follows:

(1) The incomplete decomposition of a slower reacting explosive component such as AN.

(2) The unattainment of chemical equilibrium among the detonation products from different explosive components.

We envisage the first factor to be important when the decomposition of the slowest reacting component is not self-propagating and terminates when the decomposition of the faster reacting components has gone to completion. We envisage the second factor to be important when the time scale for the detonation products to mix and react exceeds the time scales for the decomposition reactions. The constitutive relationship for reacting composite explosive used in a treatment of nonideal detonation must include enough reaction coordinates to account for nonideality arising from factors (1) and (2).

The theoretical model for nonideal detonation presented in this report was formulated to provide a better understanding and a means for approaching the problem of steady-state detonation in composite explosives. With X_1, X_2, and X_3 considered, respectively, to be like RDX, TNT, and AN, it was necessary to construct a constitutive relationship for the reacting explosive with the four reaction coordinates λ_1, λ_2, λ_3, and λ_4. The first three coordinates account respectively for the global decompositions of X_1, X_2, and X_3, and the fourth accounts for the recombination of the oxygen produced by X_3 and the carbon produced by X_1 and X_2. This constitutive relationship, the RH jump conditions, and the CJ sonic condition were combined to generate the equations governing the steady reaction zone and thereby demonstrate the dependence of the detonation process in composite explosives on incomplete reaction and on the equation of state of the condensed explosive. The expression relating the particle velocity and the reaction coordinates in a steady-state reaction zone was also derived. This expression was combined with model reaction rate expressions to generate Lagrange particle velocity histories and to investigate the dependence of particle velocity on the relative rates of the exothermic reactions.

Governing Equations

Flow Equations

We first introduce the notation used to describe our one-dimensional flow. Time is denoted by t, Lagrange distance by h, specific volume by v,

particle velocity by u, pressure by p, sound speed by c, and specific energy by e; the subscript x denotes explosive, and the superscript o denotes the constant state ahead of the wave. Neglecting the initial pressure, the flow in our steady-state ZND wave is governed by the RH jump conditions written as

$$vD = v_x^o (D - u) \tag{1}$$

$$p = Du/v_x^o = (D - u)u/v \tag{2}$$

$$e - e_x^o = \frac{1}{2} p \left(v_x^o - v\right) = \frac{1}{2} u^2 \tag{3}$$

where D denotes the propagation velocity. We use H as a subscript or as a superscript to denote the shocked state at the wave front, and we use CJ as a subscript to denote the CJ point. Then the equations for the shocked state are obtained by setting $v = v_x^H$, $u = u_H$, $p = p_H$, and $e = e_x^H$ in Eqs. (1)-(3), and the equations for the CJ state are obtained by writing the CJ condition as

$$D - u_{CJ} = c_{CJ} \tag{4}$$

and setting $v = v_{CJ}$, $u = u_{CJ}$, $p = p_{CJ}$, and $e = e_{CJ}$ in Eqs. (1)-(3). The adiabatic inviscid flow in the wave behind the shock is governed by the following expressions for the laws of conservation of mass, momentum, and energy:

$$\frac{\partial v}{\partial t} = v_x^o \frac{\partial u}{\partial h} = - D \frac{\partial v}{\partial h} \tag{5}$$

$$\frac{\partial u}{\partial t} = - v_x^o \frac{\partial p}{\partial h} = - D \frac{\partial u}{\partial h} \tag{6}$$

$$\frac{\partial e}{\partial t} = - p \frac{\partial v}{\partial t} \tag{7}$$

The flow and chemistry in our ZND wave are coupled by the constitutive relationship relating e and the reaction coordinates λ_1, λ_2, λ_3 and λ_4.

Equations for the Explosive

Following the papers by Kamlet et al.,[2-4] we write the molecular formulas of our explosive components X_1, X_2, and X_3, respectively, as $C_{a_i} H_{b_i} N_{c_i} O_{d_i}$ with i = 1, 2, and $H_{b_3} N_{c_3} O_{d_3}$. We also assume that the decompositions of X_1 and X_2 satisfy the H_2O - CO_2 arbitrary equilibrium condition. The H_2O - CO_2 arbitrary represents N_2, H_2O, and CO_2 as being the only important detonation products, with H_2O having priority in formation over CO_2. We accordingly write the decomposition of X_i, with i = 1, 2, as

$$C_{a_i} H_{b_i} N_{c_i} O_{d_i} \rightarrow \frac{c_i}{2} N_2 + \frac{b_i}{2} H_2O + \left(\frac{d_i}{2} - \frac{b_i}{4}\right) CO_2 + \left(a_i - \frac{d_i}{2} + \frac{b_i}{4}\right) C \qquad (8)$$

Extending the notion, we assume that the decomposition of X_3 satisfies the H_2O - O_2 arbitrary so that N_2, H_2O, and O_2 are the only detonation products, with H_2O having priority in formation over O_2. We accordingly write the decomposition of X_3 as

$$H_{b_3} N_{c_3} O_{d_3} \rightarrow \frac{c_3}{2} N_2 + \frac{b_3}{2} H_2O + \left(\frac{d_3}{2} - \frac{b_3}{4}\right) O_2 \qquad (9)$$

The reaction coordinates λ_1, λ_2, and λ_3 are used to describe the decompositions specified by Eqs. (8) and (9), and the reaction coordinate λ_4 is used to describe the reaction

$$\left(\frac{d_3}{2} - \frac{b_3}{4}\right) O_2 + \left(\frac{d_3}{2} - \frac{b_3}{4}\right) C = \left(\frac{d_3}{2} - \frac{b_3}{4}\right) CO_2 \qquad (10)$$

with

$$(d_{3/2} - b_{3/4}) \leq \sum_{i=1}^{2} (a_i - d_{i/2} + b_i/4)$$

that may occur among the decomposition products of X_1, X_2, and X_3. Because of the H_2O - CO_2 and H_2O - O_2 arbitrary assumptions, only one

reaction coordinate is needed to account for subsequent reactions among detonation products. With the standard heat of formation of a species S_j denoted by $(\Delta H_f^o)_{S_j}$, the standard heats, Q_i, liberated in our exothermic reactions Eqs. (8)-(10) are given by the equations

$$Q_i = -(b_i/2)\ (\Delta H_f^o)_{H_2O} - (d_i/2 - b_i/4)\ (\Delta H_f^o)_{CO_2} + (\Delta H_f^o)_{X_i} \tag{11}$$

with i = 1, 2

$$Q_3 = -(b_3/2)\ (\Delta H_f^o)_{H_2O} + (\Delta H_f^o)_{X_3} \tag{12}$$

$$Q_4 = -(d_3/2 - b_{3/4})(\Delta H_f^o)_{CO_2} \tag{13}$$

where $(\Delta H_f^o)_{H_2O} = -57.8$ kcal/mole and $(\Delta H_f^o)_{CO_2} = -94$ kcal/mole. We now introduce the notation used to describe our explosive mixture and its reaction products. We let the subscript p denote detonation products, let M_{S_j} denote the molecular weight of a product species S_j, and we let $v_{x_i}^o$, $e_{x_i}^o$, N_i, and α_i denote the initial specific volume, the initial specific internal energy, the number of moles, and the mass fraction of the explosive X_i in our composite explosive X. Then N_i and α_i are related by the equation

$$N_i = \alpha_i/M_{x_i} \qquad i = 1, \ldots 3 \tag{14}$$

With $\sum_{i=1}^{3} N_i M_{x_i} = 1$. We assume that the mixture of explosives is ideal and write the following equations for its specific volumes, specific internal energy, and specific heat of formation:

$$v_x^o = \sum_{i=1}^{3} \alpha_i\ v_{x_i}^o \tag{15}$$

$$e_x^o = \sum_{i=1}^{3} \alpha_i\ e_{x_i}^o \tag{16}$$

$$(\Delta h_f^o)_x = \sum_{i=1}^{3} \alpha_i \, (\Delta h_f^o)_{x_i} \tag{17}$$

where $(\Delta h_f^o)_{S_j} = (\Delta H_f^o)_{S_j} / M_{S_j}$. If we assume that the initial pressure is zero, Eqs. (16) and (17) are identical because $(\Delta h_f^o)_{x_i} = e_{x_i}^o$. We let $\beta_{S_j}^i$ denote the mass fraction of a decomposition product, S_j, of X_i when X_i has decomposed completely. Then under the $H_2O - CO_2$ and H_2O arbitrary assumptions it follows from Eqs. (8) and (9) that

$$\beta_{N_2}^i + \beta_{H_2O}^i + \beta_{CO_2}^i + \beta_C^i = 1 \qquad i = 1, 2 \tag{18}$$

and

$$\beta_{N_2}^3 + \beta_{H_2O}^3 + \beta_{O_2}^3 = 1 \tag{19}$$

where

$$\beta_{N_2}^i = c_i M_{N_2} / 2M_{x_i} \qquad i = 1, 2, 3$$

$$\beta_{H_2O}^i = b_i M_{H_2O} / 2M_{x_i} \qquad i = 1, 2, 3;$$

$$\beta_{CO_2}^i = (d_i - b_i/2) \, M_{CO_2} / 2M_{x_i} \qquad i = 1, 2;$$

$$\beta_C^i = [2a_i - (d_i - b_i/2)] \, M_C / 2M_{x_i} \qquad i = 1, 2;$$

$$\beta_{O_2}^3 = (d_3 - b_3/2) \, M_{O_2} / 2M_{x_3}$$

We can then write the standard heats $\hat{q}_1$, $\hat{q}_2$, and $\hat{q}_3$ liberated by the decomposition of 1 gram of X_1, X_2, and X_3 as

$$\hat{q}_i = - \beta_{H_2O}^i (\Delta h_f^o)_{H_2O} - \beta_{CO_2}^i (\Delta h_f^o)_{CO_2} + (\Delta h_f^o)_{x_i} \qquad i = 1, 2 \tag{20}$$

$$\hat{q}_3 = -\beta^3_{H_2O}\,(\Delta h^o_f)_{H_2O} + (\Delta h^o_f)_{x_3} \tag{22}$$

and the standard heat $\hat{q}_d$ liberated by the decomposition of X_1, X_2, and X_3 in 1 gram of X as

$$\hat{q}_d = \sum_{i=1}^{3} \alpha_i \hat{q}_i \tag{22}$$

We now consider the reaction among the detonation products, Eq. (10), and write the standard heat of this reaction for 1 gram of X_3 as

$$\hat{q}_4 = \beta^4_{CO_2}\,(\Delta h^o_f)_{CO_2} \tag{23}$$

where $\beta^4_{CO_2} = (d_3/2 - b_3/4)\, M_{CO_2}/M_{x_3}$. Thus, when all the exothermic reactions proceed to completion in our composite explosive, we can write the standard heat of these reactions for 1 gram of X as

$$\hat{q} = \sum_{i=1}^{3} q_i + q_4 \tag{24}$$

where $q_1 = \alpha_1\hat{q}_1$, $q_2 = \alpha_2\hat{q}_2$, $q_3 = \alpha_3\hat{q}_3$, and $q_4 = \alpha_3\,\hat{q}_4$.

Constitutive Relationship for Reacting Composite Explosive

Our constitutive relationship for reacting composite explosive is an extension of the constitutive relationship formulated previously[10] for an explosive with one global decomposition reaction. We treat the explosive components and their reaction products as a mixture of phases that attains mechanical but not thermal equilibrium. It is also assumed that no appreciable amount of heat is transferred into the composite explosive as the decomposition reactions propagate and consume the explosive components. In this case, the explosive components are compressed or released isentropically as the reactions proceed, and the pressure increases or decreases along a particle path.

We assume for convenience that the explosives and their products are polytropic materials, and we assume for tractability that the polytropic indices of the explosive components are equal, i.e., $K_{x_1} = K_{x_2} = K_{x_3} = K_x$, and that the polytropic index of carbon is the same as that of the other reaction products, i.e., $K_C = K_p$. In contrast to classical treatments of detonation, however, we do not assume that $K_x = K_p = K$ so that we can investigate the influence of the equation of state of the condensed explosive on the detonation process. We accordingly write the (e-p-v) relationships for the explosive components and their reaction products as

$$e_{x_i} = (\Delta h_f^o)_{x_i} + \frac{pv_{x_i}}{(K_{x_i} - 1)} \qquad i = 1, 2, 3 \tag{25}$$

$$e_p = (\Delta h_f^o)_p + \frac{pv_p}{(K_p - 1)} \tag{26}$$

We denote the specific entropy by s and write the mixture rules for the reacting explosive mixture as

$$e = \Sigma e_x + \bar{e}_p \tag{27}$$

$$v = \Sigma v_x + \bar{v}_p \tag{28}$$

$$s = \Sigma s_x + \bar{s}_p \tag{29}$$

with

$$\Sigma v_x = \sum_{i=1}^{3} \alpha_i (1 - \lambda_i)\, v_{x_i}$$

$$\Sigma s_x = \sum_{i=1}^{3} \alpha_i (1 - \lambda_i)\, s_{x_i}$$

$$\Sigma e_x = (\Delta h_f^o)_x - \sum_{i=1}^{3} \lambda_i \alpha_i (\Delta h_f^o)_{x_i} + \frac{p \Sigma v_x}{K_x - 1} \tag{30}$$

and

$$\bar{e}_p = \sum_{i=1}^{2} \lambda_i \alpha_i \beta^i_{H_2O} (\Delta h^o_f)_{H_2O} + \sum_{i=1}^{2} \lambda_i \alpha_i \beta^i_{CO_2} (\Delta h^o_f)_{CO_2}$$

$$+ \lambda_3 \alpha_3 \beta^3_{H_2O} (\Delta h^o_f)_{H_2O} + \lambda_3 \lambda_4 \alpha_3 \beta^4_{CO_2} (\Delta h^o_f)_{CO_2} + \frac{p\bar{v}_p}{(K_p - 1)} \quad (31)$$

The combination of Eqs. (27), (30), and (31) after some manipulation gives the constitutive relationship for our reacting mixture as

$$e = (\Delta h^o_f)_x - \sum_{i=1}^{3} \lambda_i q_i - \lambda_4 \lambda_3 q_4 + \frac{pv}{K_p - 1} - \frac{K_{xp} p \Sigma v_x}{K_p - 1} \quad (32)$$

with $q_i = \alpha_i \hat{q}_i$, $q_4 = \alpha_3 \hat{q}_4$, and $K_{xp} = (K_x - K_p)/(K_x - 1)$. The (e-p-v) relationship for our composite polytropic explosive is obtained from Eq. (32) by setting $\lambda_1 = \lambda_2 = \lambda_3 = 0$, $v = v_x$, and $e = e_x$, and the (e-p-v) relationship for our polytropic decomposition products is obtained from Eq. (32) by setting $\lambda_1 = \lambda_2 = \lambda_3 = 1$, $v = v_p$, and $e = e_p$. The classical (e-p-v-λ_i) equation of state for a polytropic reacting explosive mixture is obtained from Eq. (32) by setting $K_x = K_p = K$.

We now define the sound speed in our reacting mixture by the equation

$$c^2 = Kpv = -v^2 \left(\frac{\partial p}{\partial v}\right)_{s, \lambda_i} \quad (33)$$

and we then use Eqs. (28) and (29) to express Eq. (33) in a more convenient form. Differentiating Eq. (29) at constant s and λ_i leads to the equation

$$d\Sigma s_x + d\bar{s}_p = 0 \quad (34)$$

and it follows that $d\bar{s}_p = 0$ because $ds_{x_i} = 0$, $i = 1, 2, 3$ by assumption. Differenting Eq. (28) partially with respect to p at constant s and λ_i and taking account of these entropy conditions gives the equation

$$\left(\frac{\partial v}{\partial p}\right)_{s,\lambda_i} = \sum_{i=1}^{3} \alpha_i (1 - \lambda_i) \left(\frac{\partial v_{x_i}}{\partial p}\right)_{s_{x_i}} + \left(\frac{\partial \bar{v}_p}{\partial p}\right)_{\bar{s}_p,\lambda_i} \tag{35}$$

which for our polytropic materials can be rewritten after some manipulation as

$$\left(\frac{\partial p}{\partial v}\right)_{s,\lambda_i} = -\frac{K_p p}{(v - \bar{K}_{xp} \Sigma v_x)} \tag{36}$$

with $\bar{K}_{xp} = (K_x - K_p)/K_x$. The combination of Eqs. (33) and (36) gives the following equation for K

$$K = \frac{K_p v}{(v - \bar{K}_{xp} \Sigma v_x)} \tag{37}$$

which reduces to $K = K_x$ when $\lambda_1 = \lambda_2 = \lambda_3 = 0$ and $v = v_x$, and to $K = K_p$ when $\lambda_1 = \lambda_2 = \lambda_3 = 1$. The assumption that an explosive component is released down its own isentrope allows us to express the Σv_x term in terms of pressure in a ZND wave. Because the explosive components are polytropic, their specific volumes can be written as

$$v_{x_i} = v_x^o \frac{(K_x - 1)}{(K_x + 1)} \delta_i \left(\frac{p_H}{p}\right)^{1/K_x} \tag{38}$$

where $\delta_i = v_{x_i}^o / v_x^o$. Thus the equation for Σv_x in our ZND wave can be written in terms of pressure as

$$\Sigma v_x = v_x^o \frac{(K_x - 1)}{(K_x + 1)} \left(\frac{p_H}{p}\right)^{1/K_x} \sum_{i=1}^{3} \bar{\alpha}_i (1_i - \lambda_i) \tag{39}$$

where $\bar{\alpha}_i = \alpha_i \, v_{x_i}^o / v_x^o$ and $\sum_{i=1}^{3} \bar{\alpha}_i = 1$.

Nonideal Steady-State Detonation Waves

The constitutive relationship can now be combined with the Rankine-Hugoniot jump conditions and the Chapman-Jouguet conditions to generate the equations governing the CJ state in our nonideal ZND wave and to generate the equation governing particle velocity in the steady-state reaction zone.

Chapman-Jouguet Conditions

We set $(\lambda_i)_{CJ} = \hat{\lambda}_i$ at the CJ point in our steady-state ZND wave. Then we can represent ideal detonation by the set $\{\hat{\lambda}_1 = 1, \hat{\lambda}_2 = 1, \hat{\lambda}_3 = 1, \hat{\lambda}_4 = 1\}$ and nonideal detonation by the set $\{\hat{\lambda}_1, \hat{\lambda}_2, \hat{\lambda}_3, \hat{\lambda}_4\}$ with any one of the reaction coordinates satisfying the condition $\hat{\lambda}_i < 1$. In the present case, we assume that the RDX-like component X_1 and the TNT-like component X_2 decompose completely, and represent our nonideal detonation by the set $\{\hat{\lambda}_1 = 1, \hat{\lambda}_2 = 1, \hat{\lambda}_3 < 1, \hat{\lambda}_4 < 1\}$. We are therefore going to consider incomplete decomposition of the AN-like component and incomplete reaction among the carbon from X_1 and X_2 and the oxygen from X_3.

We first combine Eqs. (2), (4), and (33) to obtain the following relationship between sound speed and particle velocity at the CJ point:

$$c_{CJ} = \hat{K}\, u_{CJ} \tag{40}$$

where

$$\hat{K} = \frac{K_p}{\left(1 - \bar{K}_{xp}\Sigma\hat{v}_x/v_{CJ}\right)} \tag{41}$$

with $\Sigma\hat{v}_x = \alpha_3(1 - \hat{\lambda}_3)(v_{x_3})_{CJ}$. Combining Eq. (40) with Eqs. (4) and (1) then gives the equations

$$u_{CJ} = \frac{D}{\hat{K} + 1} \tag{42}$$

$$c_{CJ} = \frac{\hat{K}\, D}{\hat{K} + 1} \tag{43}$$

and

$$v_{CJ} = \frac{\hat{K}}{\hat{K} + 1} v_x^o \tag{44}$$

The equation

$$\left[\left(\frac{\partial p}{\partial v}\right)_{s, \lambda_i}\right]_{CJ} = - \frac{p_{CJ}}{v_x^o - v_{CJ}} \tag{45}$$

expressing the tangency condition of the isentrope and the Rayleigh line at the CJ point is then used to obtain the following equations for the specific volume at the CJ point:

$$\frac{v_{CJ}}{v_x^o} = \frac{K_p}{K_p + 1} + \frac{\bar{K}_{xp}}{K_p + 1} \frac{\Sigma \hat{v}_x}{v_x^o} \tag{46}$$

$$1 - \frac{v_{CJ}}{v_x^o} = \frac{\left(1 - \bar{K}_{xp} \Sigma \hat{v}_x / v_x^o\right)}{K_p + 1} \tag{47}$$

The combination of Eqs. (44) and (47) then gives the following equation relating the polytropic indices at the CJ point:

$$\hat{K} + 1 = \frac{K_p + 1}{1 - \bar{K}_{xp} \Sigma \hat{v}_x / v_x^o} \tag{48}$$

The equation relating the CJ pressure and the shock pressure at the front of our ZND wave is obtained as

$$\frac{p_{CJ}}{p_H} = \frac{K_x + 1}{2(K_p + 1)} \left(1 - \bar{K}_{xp} \Sigma \hat{v}_x / v_x^o\right) \tag{49}$$

by combining Eq. (47), the strong shock condition

$$1 - \frac{v_H}{v_x^o} = \frac{2}{K_x + 1} \tag{50}$$

and the following equation expressing the balance of mass and momentum in a steady-state wave

$$\frac{p_{CJ}}{p_H} = \frac{(1 - v_{CJ}/v_x^o)}{(1 - v_H/v_x^o)} \tag{51}$$

The equation for the detonation velocity is obtained by combining the RH jump conditions, the constitutive relationship Eq. (32), and the CJ condition. It is convenient to set

$$\sum_{i=1}^{3} \lambda_i q_i + \lambda_3 \lambda_4 q_4 = Q \tag{52}$$

and combine Eqs. (2), (3), and (32) to obtain the following equation for the particle velocity:

$$u^2 - \frac{2Du}{K_p + 1}\left(1 - K_{xp}\Sigma v_x/v_x^o\right) = -\frac{2(K_p - 1)}{K_p + 1} Q \tag{53}$$

The CJ condition $D = (\hat{K} + 1)u_{CJ}$ then gives the following equation for u_{CJ}:

$$u_{CJ}^2\left[1 - \frac{2(\hat{K} - 1)}{K_p + 1}\left(1 - K_{xp}\hat{\Sigma v}_x/v_x^o\right)\right] = -\frac{2(K_p - 1)}{K_p + 1}\hat{Q} \tag{54}$$

where $\hat{Q} = q_1 + q_2 + \hat{\lambda}_3 (q_3 + \hat{\lambda}_4 q_4)$ because of our assumption that $\lambda_1 = \lambda_2 = 1$. Combining Eqs. (54) and (48) gives the following equation

$$u_{CJ}^2 \left[\frac{1 - \left(2K_{xp} - \bar{K}_{xp}\right) \Sigma\hat{v}_x/v_x^o}{\left(1 - \bar{K}_{xp} \Sigma\hat{v}_x/v_x^o\right)} \right] = \frac{2(K_p - 1)\hat{Q}}{K_p + 1} \tag{55}$$

which with Eqs. (44) and (48) leads to the following equation for the detonation velocity:

$$D^2 = \frac{2(K_p^2 - 1)\hat{Q}}{\left(1 - \bar{K}_{xp} \Sigma\hat{v}_x/v_x^o\right)\left[1 - \left(2K_{xp} - \bar{K}_{xp}\right)\Sigma\hat{v}_x/v_x^o\right]} \tag{56}$$

The problem of nonideal detonation in our simple treatment of detonation is that of calculating $\Sigma\hat{v}_x/v_x^o$, $\hat{\lambda}_3$, and $\hat{\lambda}_4$. It follows from Eq. (39) that the equation for $\Sigma\hat{v}_x/v_x^o$ can be written as

$$\Sigma' v_x/v_x^o = \frac{\left(K_x - 1\right)}{K_x + 1} \bar{\alpha}_3(1 - \hat{\lambda}_3) \left(\frac{P_H}{P_{CJ}}\right)^{1/K_x} \tag{57}$$

but models for calculating $\hat{\lambda}_3$ and $\hat{\lambda}_4$ must be formulated or their values must be estimated before detonation parameters can be calculated.

When a relationship between $\hat{\lambda}_3$ and $\hat{\lambda}_4$ is known, however, Eqs. (49), (57), and (56) can be used to investigate the dependence of D on $\hat{\lambda}_3$ as follows. We set $\varepsilon = \left(1 - \bar{K}_{xp} \Sigma\hat{v}_x/v_x^o\right)$, write Eq. (49) as

$$\varepsilon = \frac{2(K_p + 1)}{K_x + 1} \frac{P_{CJ}}{P_H} \tag{58}$$

so that

$$\Sigma \hat{v}_x/v_x^o = \bar{\alpha}_3(1 - \hat{\lambda}_3) \frac{K_x - 1}{K_x + 1} \left(\frac{P_H}{P_{CJ}}\right)^{1/K_x} = \frac{1 - \varepsilon}{\bar{K}_{xp}} \tag{59}$$

and assign ε a value a little less than 1. We calculate the corresponding values of p_{CJ}/p_H and $\Sigma\hat{v}_x/v_x^o$ from Eqs. (58) and (59), and then we calculate the value of $\hat{\lambda}_3$ from Eq. (59). The relationship between $\hat{\lambda}_3$ and $\hat{\lambda}_4$ gives the value of $\hat{\lambda}_4$, and the detonation velocity can then be calculated from Eq. (56).

Examination of the equations for the CJ parameters shows that the equations for complete decomposition of X_3 with $\hat{\lambda}_3 = 1$ have the same form as those for polytropic explosive with $K_{xp} = \bar{K}_{xp} = 0$. In this case, the equation for the detonation velocity reduces to

$$D^2 = 2(K_p^2 - 1)(q_1 + q_2 + q_3 + \hat{\lambda}_4 q_4) \tag{60}$$

and the nonideality arises solely from the incompleteness of the reaction among the carbon from X_1 and X_2 and the oxygen from X_3.

Dependence of Particle Velocity on Reaction Coordinates

It is convenient to use Eq. (53) to derive the relationship of the particle velocity and the reaction coordinates in a steady-state ZND wave. We write Eq. (53) to make its left-hand side into a perfect square and then combine this equation with the CJ conditions, Eqs. (42) and (48), to obtain the equation

$$\frac{u}{u_{CJ}} = \frac{(1 - K_{xp}\Sigma v_x/v_x^o)}{(1 - \bar{K}_{xp}\Sigma\hat{v}_x/v_x^o)}\left[1 + \left\{1 - \frac{2(K_p^2 - 1)Q}{(1 - K_{xp}\Sigma v_x/v_x^o)^2 D^2}\right\}^{1/2}\right] \tag{61}$$

Equation (56) then allows Eq. (61) to be written as

$$\frac{u}{u_{CJ}} = \frac{(1 - K_{xp}\Sigma v_x/v_x^o)}{(1 - \bar{K}_{xp}\Sigma\hat{v}_x/v_x^o)}\left(1 + \left\{\frac{1 - [1 - (2K_{xp} - \bar{K}_{xp})\Sigma v_x/v_x^o](1 - \bar{K}_{xp}\Sigma v_x/v_x^o)Q}{(1 - K_{xp}\Sigma v_x/v_x^o)^2 Q}\right\}^{1/2}\right) \tag{62}$$

with

$$\Sigma v_x/v_x^o = \frac{K_x - 1}{K_x + 1}\left(\frac{u_H}{u_{CJ}}\right)^{1/K_x}\left(\frac{u_{CJ}}{u}\right)^{1/K_x} \sum_{i=1}^{3} \bar{\alpha}_i(1 - \lambda_1) \tag{63}$$

from Eq. (39), and with $\lambda_1 = \lambda_2 = 1$, $\lambda_3 = \hat{\lambda}_3$, and $\lambda_4 = \hat{\lambda}_4$ at the CJ point where $Q = \hat{Q}$, $\Sigma v_x = \hat{\Sigma v}_x$, and $u = u_{CJ}$. The equation for the particle velocity in a steady-state ZND wave when X_3 decomposes completely is obtained by setting $\hat{\lambda}_3 = 1$ in Eq. (62) as

$$\frac{u}{u_{CJ}} = \left(1 - K_{xp}\Sigma v_x/v_x^o\right)\left[1 + \left\{1 - \frac{Q}{\left(1 - K_{xp}\Sigma v_x/v_x^o\right)^2 \hat{Q}_d}\right\}^{1/2}\right] \tag{64}$$

where $\hat{Q}_d = q_1 + q_2 + q_3 + \hat{\lambda}_4 q_4$. The equation for the particle velocity in a steady-state ZND wave in polytropic explosive is obtained from Eq. (62) by setting $K_{xp} = \bar{K}_{xp} = 0$ and is conveniently written as

$$\frac{u}{u_{CJ}} = 1 + \left[\tilde{\alpha}_1(1 - \lambda_1) + \tilde{\alpha}_2(1 - \lambda_2) + \tilde{\alpha}_3(1 - \lambda_3/\lambda_3) + \tilde{\alpha}_4(1 - \lambda_4/\hat{\lambda}_4)\right]^{1/2} \tag{65}$$

where

$$\tilde{\alpha}_1 = q_1/\hat{Q}$$

$$\tilde{\alpha}_2 = q_2/\hat{Q}$$

$$\tilde{\alpha}_3 = \lambda_3 q_3/\hat{Q}$$

$$\tilde{\alpha}_4 = \lambda_4 q_4/\hat{Q}$$

$$\tilde{\alpha}_1 + \tilde{\alpha}_2 + \tilde{\alpha}_3 + \tilde{\alpha}_4 = 1$$

Differentiating Eq. (53) with respect to time along a particle path gives the following equation for the deceleration in a steady-state reaction zone:

$$\frac{\partial u}{\partial t}\left[u - \frac{D(1 - \bar{K}_{xp}\Sigma v_x/v_x^o)}{(k_p + 1)}\right] = -\frac{(K_p - 1)\dot{Q}}{K_p + 1}$$

$$+ \frac{K_{xp}(K_x - 1)}{(K_p + 1)(K_x + 1)}\dot{Q}' \qquad (66)$$

where

$$\dot{Q} = q_1\frac{\partial\lambda_1}{\partial t} + q_2\frac{\partial\lambda_2}{\partial t} + (q_3 + \lambda_4 q_4)\frac{\partial\lambda_3}{\partial t} + \lambda_3 q_4\frac{\partial\lambda_4}{\partial t}$$

and

$$\dot{Q}' = \left(\frac{u_H}{u}\right)^{1/K_x} Du_i \sum_{i=1} \bar{\alpha}_i \frac{\partial\lambda_i}{\partial t} \qquad (67)$$

Because $\partial u/\partial t$ is finite, it follows in general from Eqs. (66) and (67) that the rates of all the reactions must be zero, i.e., $\partial\lambda_i/\partial t = 0$ for i = 1, 2, 3, and 4, at the sonic point where $u = u_{CJ} = D(1 - \bar{K}_{xp}\Sigma\hat{v}_x/v_x^o)/(K_p + 1)$. In other words, the CJ point is located at the end of the steady-state reaction zone of our nonideal detonation wave. The following equation,

$$u_H\left(\frac{\partial u}{\partial t}\right)_H = -\frac{2(K_p - 1)\dot{Q}_H}{K_p + 1} + \frac{K_{xp}(K_x - 1)}{K_p + 1}u_H^2 \sum_{i=1}^{3} \bar{\alpha}_i \frac{\partial\lambda_i}{\partial t_H} \qquad (68)$$

obtained by setting $u = u_H$ and $\lambda_1 = \lambda_2 = \lambda_3 = \lambda_4 = 0$ in Eq. (66), leads to the conclusion that the particle velocity will increase at the front of the wave when $K_{xp}(K_x - 1) \sum_{i=1}^{3} \bar{\alpha}_i \partial\lambda_i/\partial t_H > 2(K_p - 1)(\dot{Q}_H/u_H^2)$. Waves with this property will not, however, be considered in this report. Equations (62), (64), and (65) can be used to calculate Lagrange particle velocity histories when expressions for the reaction coordinates are known as functions of time. The Lagrange histories can then be examined to investigate the influence of the relative rates of the exothermic reactions on particle velocity. Such calculations will be presented in the next section.

Model Nonideal Detonation Calculations

Properties of the explosive X, its components X_1, X_2, and X_3, and their detonation products were chosen to model Amatex 20. We set $v_x^o = 0.6201$ cm^3/g so that the initial density $\rho_o^x = 1.613$ g/cm^3, and we assigned X_1, X_2, and X_3 the values of the parameters shown in Table 1.

We set $\hat{q}_4 = 587.5$ cal/g and $q_4 = 235$ cal/g according to Eqs. (23) and (24), and we set $K_x = 5.34$ and $K_p = 2.67$, so that $K_{xp} = 0.6152$ and $\bar{K}_{xp} = 0.5$. In this case, $q_d = \sum_{i=1}^{3} q_i$, $q_i = 951.1$ cal/g, $\hat{q}_d + q_4 = 1186.1$ cal/g, and when X_1, X_2, and X_3 decompose completely, the detonation velocity D, the shock pressure p_H, the CJ pressure p_{CJ}, and the CJ particle velocity u_{CJ} vary from values of 6.98 mm/μs, 247.7 kbar, 214 kbar, and 1.90 mm/μs to values of 7.80 mm/μs, 309.6 kbar, 267.4 kbar, and 2.12 mm/μs as $\hat{\lambda}_4$ varies from zero to one. We will now calculate detonation parameters when $\hat{\lambda}_1 = \hat{\lambda}_2 = 1$, $\hat{\lambda}_3 < 1$, and $\hat{\lambda}_4 < 1$.

Detonation Parameters

We calculate detonation parameters for a nonideal detonation with $\hat{\lambda}_3 > 1$ and $\hat{\lambda}_4 < 1$. Our calculations are based on the intuitive hypothesis that the slope of the D versus $\hat{\lambda}_3$ curve is positive as $\hat{\lambda}_3$ approaches 1 when $\hat{\lambda}_4$ is a function of λ_3. We accordingly differentiate Eq. (56) and set $dD/d\hat{\lambda}_3 > 0$ when $\hat{\lambda}_3 = 1$ to find conditions to satisfy this hypothesis. For notational simplicity, we set $\bar{K}_{xp} = K_1$ and $2K_{xp} - \bar{K}_{xp} = K_2$. Differentiating Eq. (56) with respect to $\hat{\lambda}_3$ then gives the equation

$$\frac{2}{D}\frac{dD}{d\hat{\lambda}_3} = \frac{1}{\hat{Q}}\frac{d\hat{Q}}{d\hat{\lambda}_3} + \frac{d\left(\Sigma\hat{v}_x/v_x^o\right)}{d\hat{\lambda}_3}\left[\frac{K_1 + K_2 - 2K_1K_2\Sigma v_x/v_x^o}{\left(1 - K_1\Sigma\hat{v}_x/v_x^o\right)\left(1 - K_2\Sigma\hat{v}_x/v_x^o\right)}\right] \tag{69}$$

which reduces to

$$\left.\frac{2}{D}\frac{dD}{d\hat{\lambda}_3}\right|_{\hat{\lambda}_3 = 1} = \left.\frac{q_3 + q_4\left(\hat{\lambda}_4 + d\hat{\lambda}_4/d\hat{\lambda}_3\right)}{q_1 + q_2 + q_3 + \hat{\lambda}_4 q_4}\right|_{\hat{\lambda}_3 = 1} - 2K_{xp}\bar{\alpha}_3\frac{(K_x - 1)}{(K_x + 1)}\left(\frac{2(K_p + 1)}{(K_x + 1)}\right)^{1/K_x} \tag{70}$$

Table 1

VALUES OF THE PARAMETERS FOR X_1, X_2, and X_3

X_1	α_i	$v^o_{x_i}$ (cm^3/g)	$\bar{\alpha}_i$	$\hat{q}_1$ (cal/g)	q_1 (cal/g)
X_1	0.2	0.5649	0.1821	1482.4	296.5
X_2	0.4	0.6667	0.4302	1282.8	513.1
X_3	0.4	0.6009	0.3877	353.7	141.5

when $\hat{\lambda}_3 = 1$. We set $\hat{\lambda}_4 = n\,\hat{\lambda}_3$ with $n < 1$ for simplicity so that $(dD/d\hat{\lambda}_3)_{\hat{\lambda}_{3=1}} > 0$ when

$$\frac{q_3 + 2n\,q_4}{q_1 + q_2 + q_3 + n\,q_4} > 2\,K_{xp}\,\bar{\alpha}_3\,\frac{(K_x - 1)}{(K_x + 1)}\left(\frac{2(K_p + 1)}{(K_x + 1)}\right)^{1/K_x} \qquad (71)$$

Solving this inequality for n shows that

$$\left(dD/d\hat{\lambda}_3\right)_{\hat{\lambda}_3 = 1} > 0$$

when $n > 0.454$. We are now in a position to calculate detonation parameters for specified values of n and $\hat{\lambda}_3$. We set $n = 0.6$, and use Eqs. (49), (57), (56), (48), (42), (2), and (46) to calculate values of the detonation parameters for specified values of $\hat{\lambda}_3$ as follows. Equations (49) and (57) are solved for a given value of $\hat{\lambda}_3$ to find the corresponding values of (p_H/p_{CJ}) and $\Sigma\hat{v}_x/v_x^o$. Equations (56) and (48) are then used to calculate the values of D and $\hat{K}$, and equations (42), (2), and (46) are used to calculate the values of u_{CJ}, p_{CJ} and v_{CJ}/v_x^o. Calculated values of the detonation parameters are given in Table 2.

Values of the detonation velocity are given to three figures in Table 2 to show that the detonation velocity has a minimum at $\lambda_3 \approx 0.75$, while the CJ pressure and particle velocity increase monotonically as λ_3 increases from a value of 0.45 to a value of 1. The detonation velocity exhibits a minimum because K decreases monotonically with $\hat{\lambda}_3$ as u_{CJ} increases. This minimum demonstrates the influence of the equations of state of the condensed explosives on the nonideal detonation process in composite explosives.

Table 2

DETONATION PARAMETERS FOR $\lambda_3 \leq 1$ AND $\lambda_4 = 0.6\ \lambda_3$

λ_3	D (mm/μs)	P_{CJ} (kbar)	u_{CJ} (mm/μs)	u_{CJ}/u_x^o	K	pH/P_{CJ}
0.45	7.505	228.7	1.889	0.7483	2.972	1.253
0.55	7.479	230.6	1.911	0.7444	2.913	1.234
0.65	7.464	233.1	1.936	0.7406	2.856	1.216
0.75	7.459	236.1	1.963	0.7369	2.800	1.199
0.85	7.463	239.8	1.992	0.7331	2.747	1.182
0.95	7.475	243.9	2.023	0.7294	2.695	1.166
1.00	7.484	246.2	2.039	0.7275	2.670	1.158

Lagrange Particle Velocity Histories

It is clear from Eq. (62) that expressions for time variations of the reaction coordinates λ_1, λ_2, λ_3, and λ_4 must be known before we can calculate the Lagrange particle velocity history in the reaction zone of a nonideal steady-state reaction zone. Bearing in mind that the rates of all the exothermic reactions must be zero at the CJ point, we formulated simple expressions for the reaction coordinates to perform such calculations. These expressions are based on the following equation for a reaction that proceeds to completion.

$$(1 - \lambda_i) = \left[1 - \frac{(t - \tau)}{T}\right]^{n_i} \tag{72}$$

where $n_i > 2$, the Lagrange time τ denotes the time a particle enters the wave, and the overall reaction time T denotes the time it takes a particle to travel from the shock front to the CJ plane. Equation (72) is written so that $\lambda_i = 0$ at the shock front where $t - \tau = 0$, and $\lambda_i = 1$ at the CJ point where $(t - \tau) = T$. Differentiating Eq. (72) with respect to time along a particle path gives the equation for the reaction rate as

$$\frac{\partial \lambda_i}{\partial t} = \frac{n_i}{T}\left[1 - \left(\frac{t - \tau}{T}\right)\right]^{n_i - 1} = \frac{n_i}{T}(1 - \lambda_i)^{(n_i - 1)/n_i} \tag{73}$$

and it follows from Eq. (73) that we are restricting our consideration to reactions with negligible activation energies.

We used Eq. (72) with i = 1 and i = 2 to model respectively the decomposition of X_1 and X_2. To account for the fact that the faster reacting RDX-like component X_1 may decompose completely within the reaction zone, we introduce a parameter $f > 1$ and modify Eq. (72) by setting

$$1 - \lambda_1 = \left[1 - \frac{f}{f - 1}\left(\frac{t - \tau}{T}\right)\right]^{n_1} \quad \text{for} \quad 0 < (t - \tau)/T < (f - 1)/f \tag{74}$$

and

$$\lambda_1 = 1 \quad \text{for } (t - \tau)/T > (f - 1)/f \tag{75}$$

In this case, the decomposition of X_1 is complete when $(t - \tau)/T = (f - 1)/f$; when $f = 3$, for example, the X_1 decomposition time is $2T/3$. It is clear that Eq. (74) can be written in the same form as Eq. (72) by scaling the reaction time and setting the new reaction time as $T_1 = (f - 1)\, T/f$.

To model the case when the decomposition of X_3 is not self-propagating, we simply set

$$\frac{\partial \lambda_3}{\partial t} = n_3 \frac{\partial \lambda_2}{\partial t} \tag{76}$$

with $n_3 < 1$ and $\partial\lambda_2/\partial t$ given by Eq. (73) with $i = 2$, so that the decomposition of X_3 ceases at the end of the reaction zone where it is not being supported by the decomposition of the other more energetic components. Integrating Eq. (76) gives the equation

$$\lambda_3 = n_3 \lambda_2 \tag{77}$$

and it follows that λ_3 will have a value of $\hat{\lambda}_3 = n_3$ at the end of the reaction zone where $\hat{\lambda}_2 = 1$.

To model the case when the recombination reaction of the oxygen from X_3 and the carbon from X_1 and X_2 proceeds at a lower rate than the production of the oxygen, we set

$$\frac{\partial \lambda_4}{\partial t} = n_4 \frac{\partial \lambda_3}{\partial t} = n_4 n_3 \frac{\partial \lambda_2}{\partial t} \tag{78}$$

with $n_4 < 1$, so that

$$\lambda_4 = n_4 \lambda_3 = n_4 n_3 \lambda_2 \tag{79}$$

and $\hat{\lambda}_4 = n_4\hat{\lambda}_3 = n_4 n_3$ at the end of the reaction zone where $\hat{\lambda}_2 = 1$. Equations (72), (74), (75), (77), and (79), with Eq. (53) rewritten as

$$\left(\frac{u}{u_{CJ}}\right)^2 - A\left(\frac{u}{u_{CJ}}\right)\left(1 - K_{xp}\Sigma v_x/v_x^o\right) = \left(1 - A\left(1 - K_{xp}\Sigma \hat{v}_x/v_x^o\right)\right)\frac{Q}{\hat{Q}} \qquad (80)$$

with $A = 2D/(K_p + 1)\, u_{CJ}$, were used to calculate Lagrange particle velocity histories in the reaction zone of nonideal detonation waves with $\hat{\lambda}_3 = 0.8$ and $\hat{\lambda}_4 = 0.6$. In this case, $D = 7.46$ mm/μs, $u_{CJ} = 1.977$ mm/μs, and $u_H/u_{CJ} = 1.190$; the equations for calculating values of λ_3 and λ_4 are obtained as $\lambda_3 = 0.8\ \lambda_2$ and $\lambda_4 = 0.6\ \lambda_3$ by setting $n_3 = 0.8$ and $n_4 = 0.6$ in Eqs. (77) and (79).

A Newton-Raphson method was used to calculate values of (u/u_{CJ}) from Eq. (88) throughout the reaction zone with values of λ_1 and λ_2 calculated from Eqs. (72), (74), and (75). The results of three such calculations, based on the assumption that X_1 decomposes faster than X_2, are shown graphically in Figures 1a-3a and 1b-3b. The profiles in Figures 1a and 1b, 2a and 2b, and 3a and 3b were calculated respectively with the following sets of parameters: $\{n_1 = 3,\ f = 4,\ n_2 = 2\}$, $\{n_1 = 2,\ f = 3,\ n_2 = 2\}$, and $\{n_1 = 3,\ f = 3,\ n_2 = 3\}$.

Differentiating Eq. (66) partially again with respect to t shows in general that $(\partial u/\partial t)_{CJ} < 0$ when $(\partial^2\lambda_2/\partial t^2)_{CJ} > 0$, and that $(\partial u/\partial t)_{CJ} = 0$ when $(\partial^2 \lambda_2/\partial t^2)_{CJ} = 0$ when λ_1, λ_3 and λ_4 are governed by Eqs. (74), (76), and (78). Examination of the particle velocity histories shows that three conditions are satisfied because $(\partial u/\partial t)_{CJ} < 0$ in Figures 1a and 2a where $n_2 = 2$ and $(\partial^2\lambda_2/\partial t^2)_{CJ} > 0$, and $(\partial u/\partial t)_{CJ} = 0$ in Figure 3a where $n_2 = 3$ and $(\partial^2\lambda_2/\partial t^2)_{CJ} = 0$. Further examination of Figures 1a-3a show that detailed properties of the Lagrange particle velocity history depend on the equations of state of the explosive and the detonation products as well as the energy release rate. However, the qualitative features of the particle velocity history are governed by the energy release rate, as shown by the observations that (1) the history calculated with ($n_1 = 3$, $n_2 = 2$) is generally steeper than the history calculated with ($n_1 = 2$,

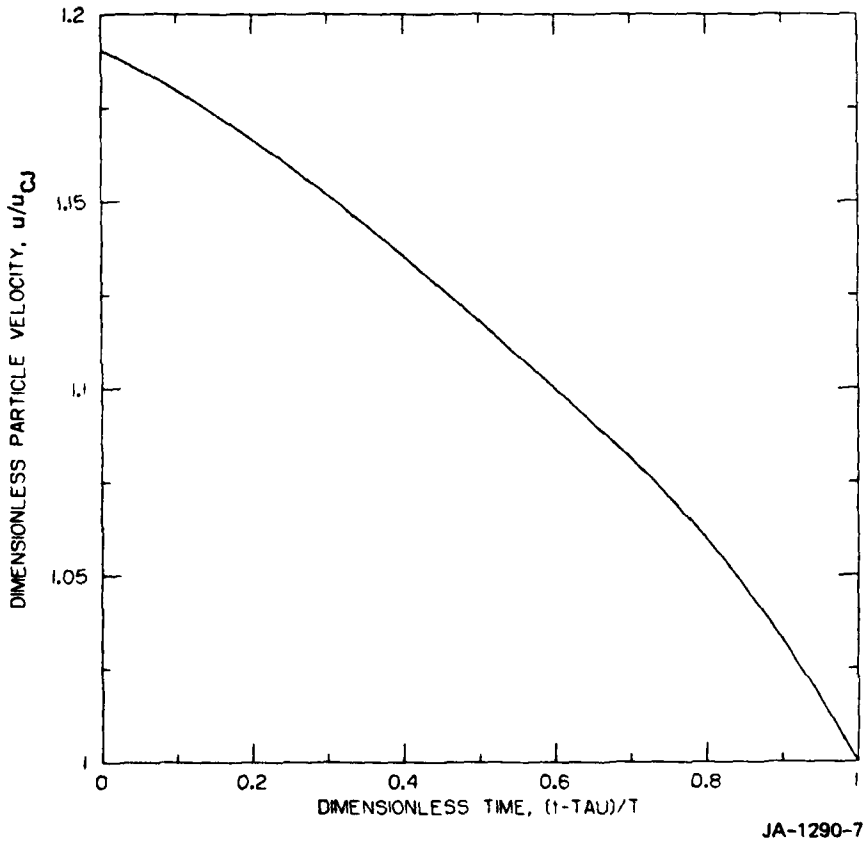

FIGURE 1a PARTICLE VELOCITY vs TIME IN REACTION ZONE CALCULATED WITH $n_1 = 3$, $f = 4$, AND $n_2 = 2$

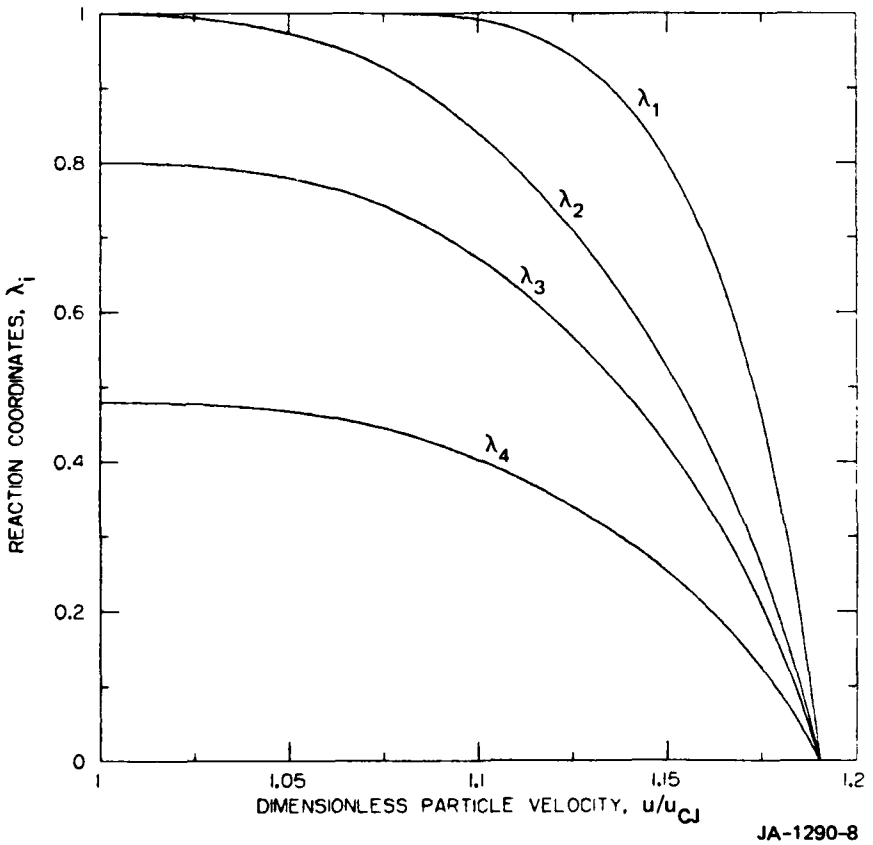

FIGURE 1b REACTION COORDINATES vs PARTICLE VELOCITY IN REACTION ZONE CALCULATED WITH $n_1 = 3$, $f = 4$, AND $n_2 = 2$

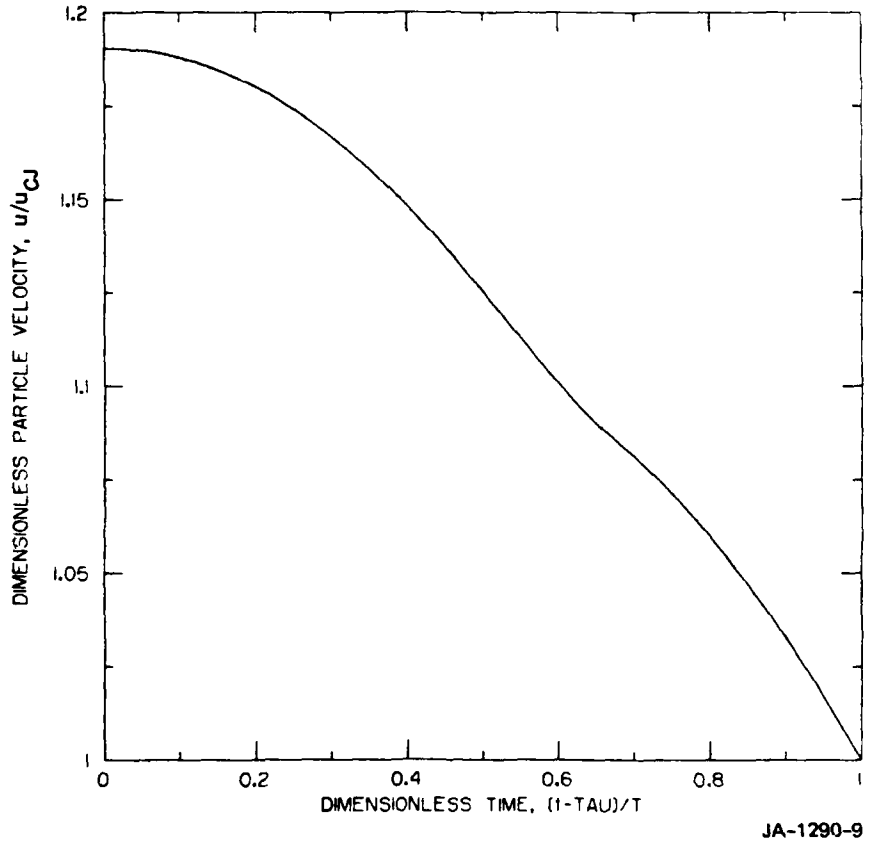

FIGURE 2a PARTICLE VELOCITY vs TIME IN REACTION ZONE CALCULATED WITH $n_1 = 2$, $f = 3$, and $n_2 = 2$

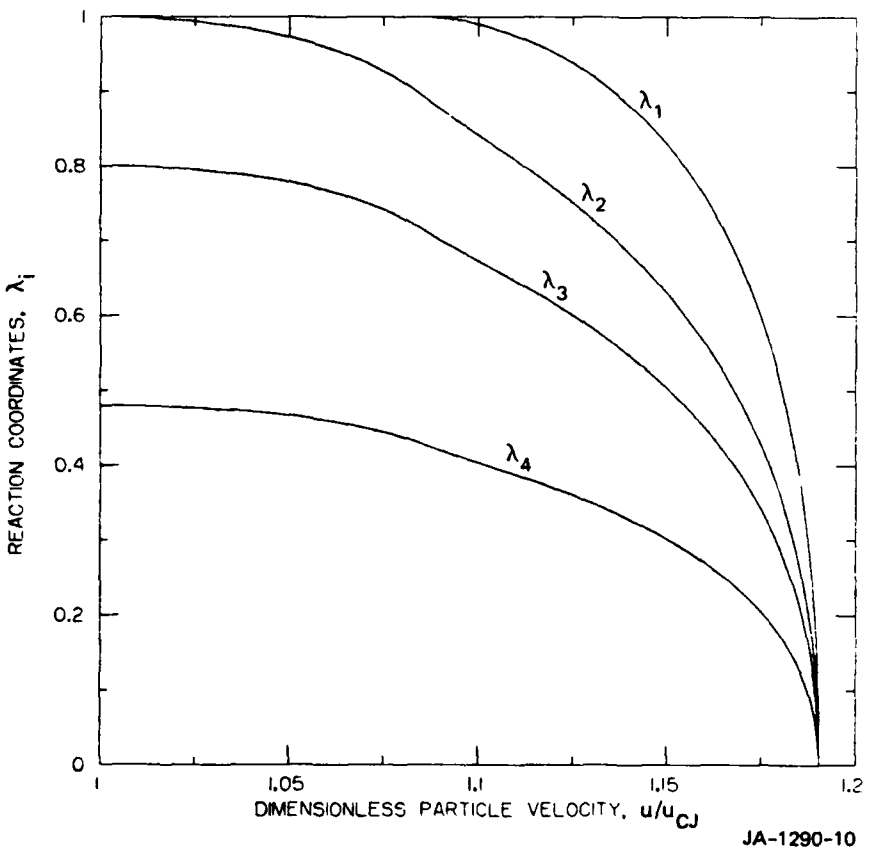

FIGURE 2b REACTION COORDINATES vs PARTICLE VELOCITY IN REACTION ZONE CALCULATED WITH $n_1 = 2$, $f = 3$, and $n_2 = 2$

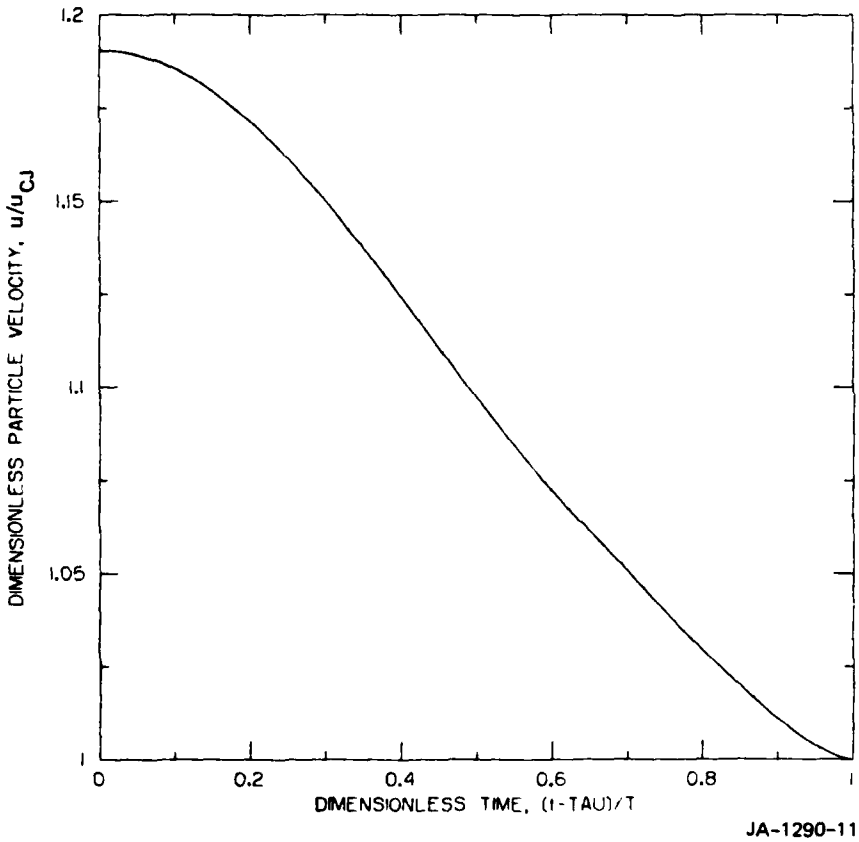

FIGURE 3a PARTICLE VELOCITY vs TIME IN REACTION ZONE CALCULATED WITH $n_1 = 3$, $f = 3$, AND $n_2 = 3$

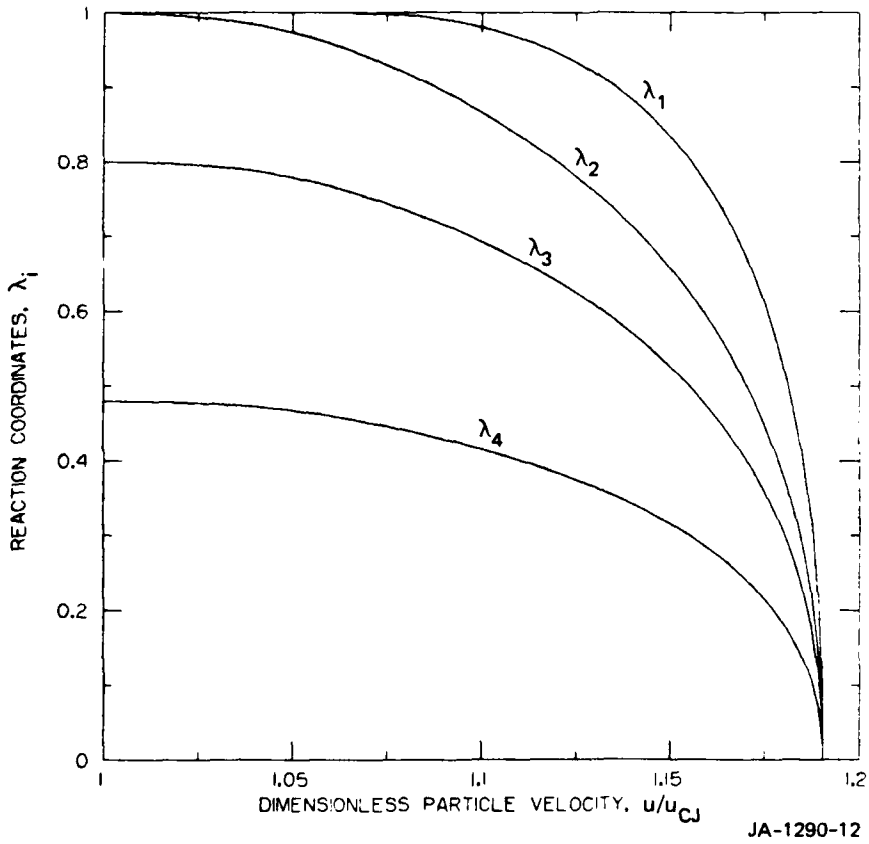

FIGURE 3b REACTION COORDINATES vs PARTICLE VELOCITY IN REACTION ZONE CALCULATED WITH $n_1 = 3$, $f = 3$, AND $n_2 = 3$

$n_2 = 2$), and (2) the history calculated with ($n_1 = 3$, $n_2 = 2$) is generally steeper than the history calculated with ($n_1 = 3$, $n_2 = 2$).

Conclusions

We have formulated a treatment of steady-state detonation waves in composite explosives. Our formulation extends the classical ZND model for ideal detonation into a prototype model for nonideal detonation. The consititutive relationship used to describe shocked reacting explosive is based on the assumption that the explosive and its detonation products are governed by different mechanical equations of state and attain mechanical, but not thermal, equilibrium. The kinetic processes responsible for nonideal behavior are assumed to be incomplete decomposition of the slowest reacting explosive component and the incomplete attainment of chemical equilibrium among the detonation products from the different explosive components.

To make our model applicable to Amatex 20, we considered a composite explosive containing an RDX-like component X_1, a TNT-like component X_2, and an AN-like component X_3. In this case the constitutive relationship must include four reaction coordinates: λ_1, λ_2, and λ_3 describe the decomposition of X_1, X_2, and X_3; λ_4 describes the reaction of the oxygen produced by X_3 and the carbon produced by X_1 and X_2. The reaction coordinates at the end of the reaction zone, $\hat{\lambda}_1$, $\hat{\lambda}_2$, $\hat{\lambda}_3$, and $\hat{\lambda}_4$, satisfy the conditions $\hat{\lambda}_1 = \hat{\lambda}_2 = \hat{\lambda}_3 = \hat{\lambda}_4 = 1$ in an ideal detonation wave, and satisfy the conditions $\hat{\lambda}_1 = \hat{\lambda}_2 = 1$, $\hat{\lambda}_3 \leq 1$, and $\hat{\lambda}_4 < 1$ in a nonideal detonation wave.

The consititutive relationship was combined with the Rankine-Hugoniot jump conditions and the CJ sonic condition to obtain the equations for the CJ parameters at the end of the reaction zone in a steady-state nonideal detonation wave. The equation governing particle velocity was combined with the CJ condition, relating particle velocity and detonation velocity in a nonideal detonation wave, to obtain the equation relating the detonation velocity to the chemical energy released in the wave. These equations for nonideal detonation specify the dependence of

the detonation parameters on the reaction coordinates and demonstrate that the detonation process is influenced by the equation of state of the explosive. Detonation calculations, using explosive parameters chosen to model Amatex 20, were performed with values of λ_3 in the range $0.45 \leq \lambda_3 \leq 1$ and $\hat{\lambda}_4 = 0.6\ \hat{\lambda}_3$ to investigate the dependence of nonideal detonation parameters on the degree of incomplete decomposition of the explosive. Simplistic reaction rate functions were also constructed and used to calculate Lagrange particle velocity histories in nonideal detonation waves.

We conclude that the result of our theoretical study is a well-formulated model for steady-state detonation that provides us with a better understanding of nonideal detonation. However, we are still faced with the major problem of formulating a realistic treatment of the decomposition of AN and subsequent reactions among the detonation products. Before the present model of nonideal detonation can be used to calculate realistic nonideal detonation parameters, we must incorporate (1) models for these kinetics processes that predict values of $\hat{\lambda}_3$ and $\hat{\lambda}_4$; and (2) more realistic equations of state.

III EXPERIMENTS

Basic Technique

The Lagrange* gage and analysis method used in this work is based on the experimental measurement of Lagrangian particle velocity histories within an explosive target undergoing planar detonation. Our experimental techniques have been described previously[1,11,12] and are summarized here.

The experimental configuration is shown in Figure 4. A target in the form of a right circular cylinder, typically about 0.2 m (8 inches) in diameter and 0.13 m (5 inches) high, is constructed from the explosive to be characterized. A plane-wave-initiated high explosive charge loads the target with a pulse of the desired amplitude and shape. Particle velocity histories are recorded at several Lagrange positions (depths) in the target for several microseconds using embedded electromagnetic particle velocity (EPV) gages.[13,14] Expendable Helmholtz coils wound on plywood frames provide a uniform quasi-static uniaxial magnetic induction in the region of the EPV gages. The gages, targets, and data are described below.

EPV Gages

Basic Operation

EPV gages are based on the principle that an electrical conductor moving in a fixed magnetic field will generate a motional electromotive force (EMF) proportional to its velocity. If the conductor, motion, and magnetic induction are each uniaxial and mutually orthogonal, as in the present case, then by Faraday's law of induction for moving circuits

---

*The term Lagrange refers to an observation made at a specific material element in the flow.

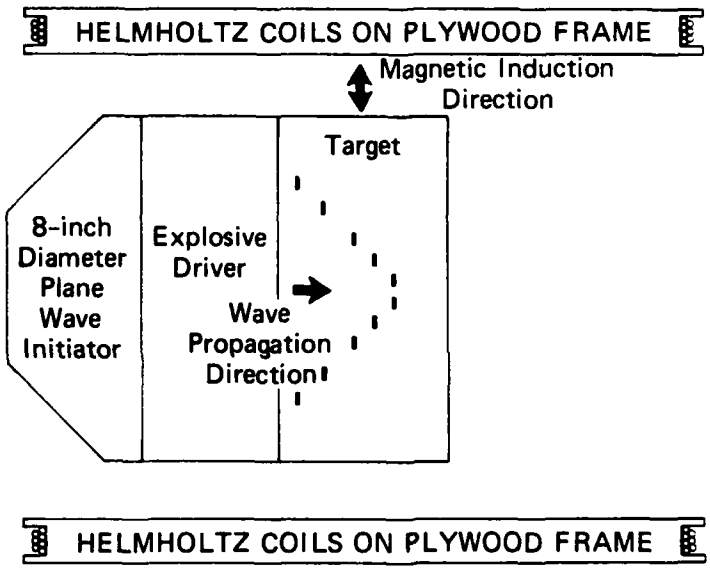

FIGURE 4 BASIC CONFIGURATION OF LARGE-SCALE LAGRANGE PARTICLE VELOCITY GAGE EXPERIMENTS

The vertical lines in the target represent cross sections of the active elements of individual embedded electromagnetic particle velocity gages; ten gages are indicated.

$$E(t) = B\ell u(t) \tag{81}$$

where E is the EMF, t is time, B is the magnitude of the magnetic induction, ℓ is the length of the conductor, and u is the velocity of the conductor.

The EPV gages used in this work were formed from aluminum strips nominally 0.15 mm thick and 3 mm wide. The strips were bent into the rectilinear U-shape shown in Figure 5. The crossbar of the U is the active element of the gage and is nominally 25.4 mm long. The sides of the U serve as electrical leads that carry the signal out the back of the target; these leads do not contribute to the signal because they are strictly parallel to the direction of motion in the target. As in our previous work,[1,11,12] the gages were not insulated because their cross-sectional area was assumed to be great enough to result in a low internal gage resistance compared with alternative conductive paths in the reaction products. After a ringup time of about 0.1 μs, the gages are estimated to reach mechanical equilibrium with the surrounding flow so that u(t) is equal to the local particle velocity.

The gage outputs, E(t), were determined from the potential drop across viewing resistors connected to the gages in simple series circuits. Standard high-frequency circuit components, consisting of shielded RG213 or RG58 coaxial cables, the viewing resistors, and Tektronix 7000 Series oscilloscopes or Nicolet digital oscilloscopes, were used in measuring the potential drops. The oscilloscopes were operated in normal (single-ended), rather than differential, mode. Because the resistance of the gages and cables was small compared with the viewing resistance, E(t) was taken to be equal to the recorded potential drops. In this work B was about 450 gauss, and the peak particle velocities were approximately 2 mm/μs, so E_{max} was greater than 2 volts and presented no recording problems. Analog oscilloscope time-bases were operated at either 500 or 1000 ns/cm and were time-correlated to less than 50 ns. Oscilloscope voltage and time calibrations were checked at the beginning and conclusion of each shot sequence.

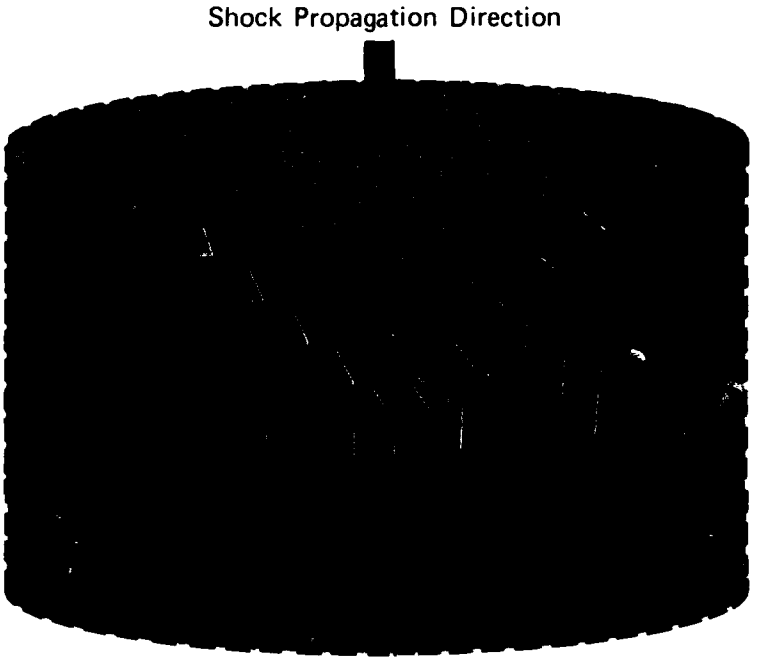

JP-1290-1

FIGURE 5 GAGE BLOCK USED TO CAST EPV GAGES INTO EXPLOSIVE TARGETS

The gage block shown contains ten gages. The configuration of the target to be cast around it is indicated by the dashed lines.

Emplacement

The gages were mounted on blocks and embedded in the targets during casting, as indicated in Figure 5. The gage blocks, machined from linen-phenolic, each contained ten gages. The blocks were secured to the bottom of cylindrical molds, and the explosive was cast around the assemblies so that the gages were not disturbed. Gage positions in the completed targets were checked radiographically, and no displacements were detected. Gage stability during explosive casting was also demonstrated in a previous program in which a gage block was embedded in an explosive simulant mixed to the efflux viscosity of an Amatex 20 explosive and then destructively sampled.[1] Casting, machining, and x-raying of the explosives were performed in the M-1 Group of Los Alamos National Scientific Laboratories (LANSL) under the direction of A. P. Torres and J. Sanchez.

Targets

Coarse-Grained Amatex 20

The variation of composition and density in the coarse-grained Amatex 20 targets was determined at LANSL from corings of a quality-control casting.

As reported by LANSL, the coring pattern is shown in Figure 6, and the Amatex 20 composition and density and the ammonium nitrate prill particle size are given in Tables 3 and 4.

Target Configuration

Standardized gage block assemblies and target dimensions were used in the Lagrange gage experiments. Figure 7 shows the configuration and the gage numbering system and gives the nominal target size and gage block position to the nearest millimeter.

The gage locations in the axial (wave propagation) direction were controlled to high precision. Each block contained two sets of five identically positioned gages (numbered 1 through 5 and 6 through 10 as

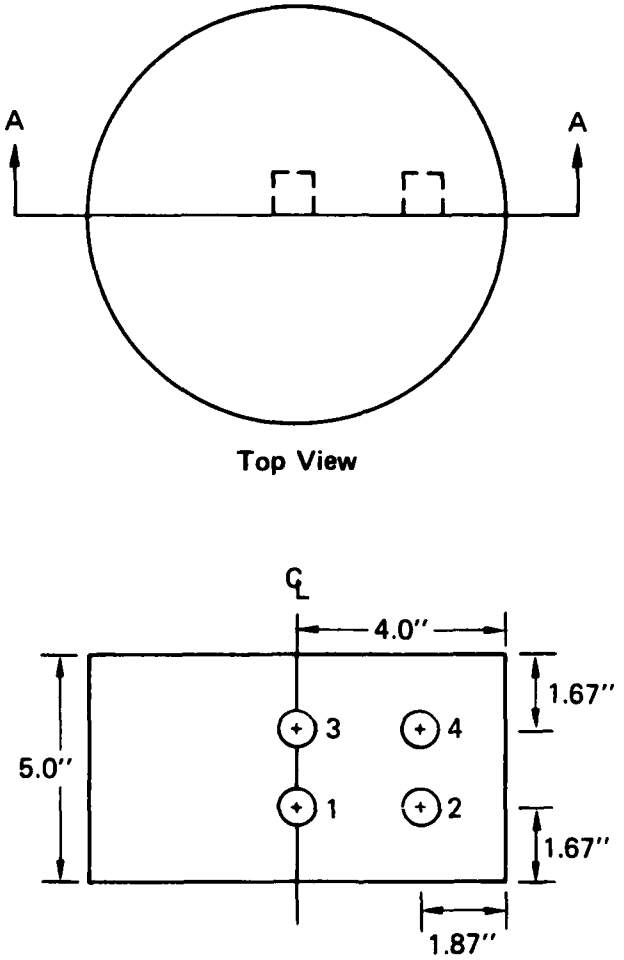

FIGURE 6 CORE PATTERN FOR COARSE-GRAINED AMATEX-20

Table 3

COARSE-GRAINED AMATEX 20 COMPOSITION AND DENSITY

Core No.	Composition (wt%) RDX	AN	TNT	Density (g/cm^3)
1	19.47	41.22	39.31	1.607
2	21.19	42.04	36.77	1.571
3	18.67	41.89	39.44	1.603
4	17.62	42.40	39.98	1.572
Average:	19.24	41.88	38.88	1.588
Spread:	3.57	1.18	3.21	0.036

Table 4

AMMONIUM NITRATE PRILL PARTICLE SIZE,
COARSE-GRAINED AMATEX 20

Mesh Size (μm)	Cumulative Percent Retained
2800	0
2000	22.0
1700	62.4
1400	88.3
1000	98.7
710	100.0

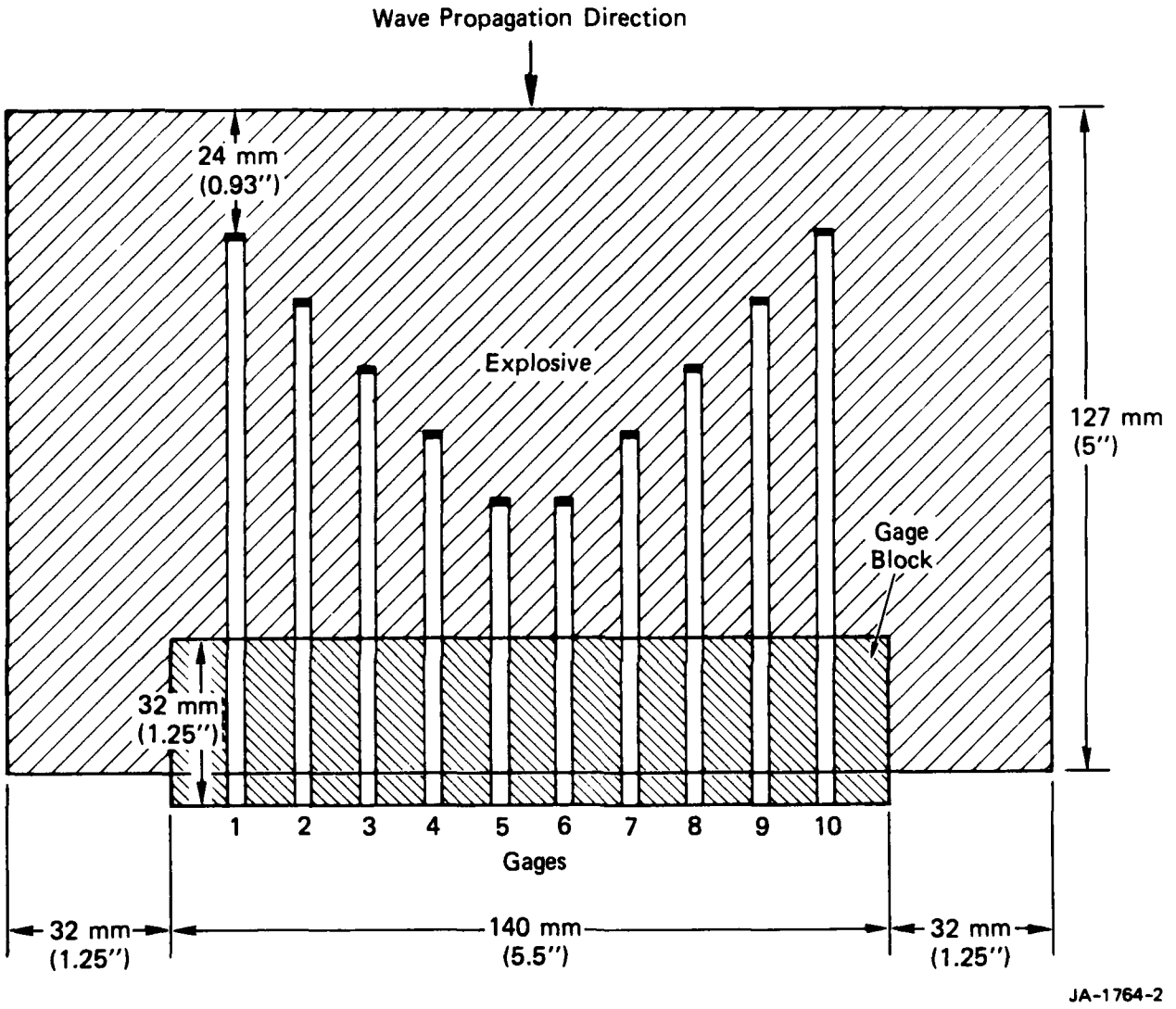

FIGURE 7 TARGET CONFIGURATION AND DIMENSIONS

A side view of the cylindrical target is shown. The gages are numbered sequentially as indicated, so, for example, 4 and 7 are in the same plane. The locations of the active elements of the gages are indicated by heavy lines.

shown in Figure 7). Thus there were two gages in each of five planes parallel to the initiating plane. The nominal distance from the initiating plane (front surface of target) to the first gage plane was 24 mm (0.93 inch); the distance between successive gage planes, used in the analysis, was 12.7 ± 0.1 mm. The lateral distance (center to center) between adjacent gages was 12.0 mm ± 0.2 mm.

Data

Two experiments were performed with coarse-grained Amatex 20. A 203-mm-diameter (8-inch) P-80 plane wave lens in contact with a 1-inch by 8-inch pad of Composition B was used to initiate the Amatex 20 target in the first experiment. A 203-mm-diameter (8-inch) P-80 plane wave lens in contact with a 1-inch by 8-inch pad of TNT was used to initiate the Amatex 20 target in the second experiment. Particle velocity records were obtained in both experiments. All high-resolution gage records except 5 and 6 were obtained with Tektronix 7844 dual-beam oscilloscopes; high resolution records for gages 5 and 6 were recorded on Tektronix 7704A single-beam oscilloscopes. The oscilloscope sensitivities for the high-resolution records were 500 mV/cm, vertical, and 500 ns/cm, horizontal. A beam intensity modulation system was used to simultaneously generate several short blanks on all the high resolution oscilloscope records. The blanks permited the individual gage records to be correlated on an absolute time-scale.

The gage records obtained in the first experiment with the Composition B driver are not included here because they show that the detonation wave in coarse-grained Amatex 20 was overdriven. The as-recorded EPV gage profiles obtained in the second experiment with the TNT driven are shown in Figure 8. These records are the basis for the Lagrange analysis presented in the next section.

Two features of the records pertaining to the experimental procedures are discussed here. First, high frequency oscillations are present on most gage records during or just after the initial acceleration of that gage. The amplitude of the oscillations decreases with

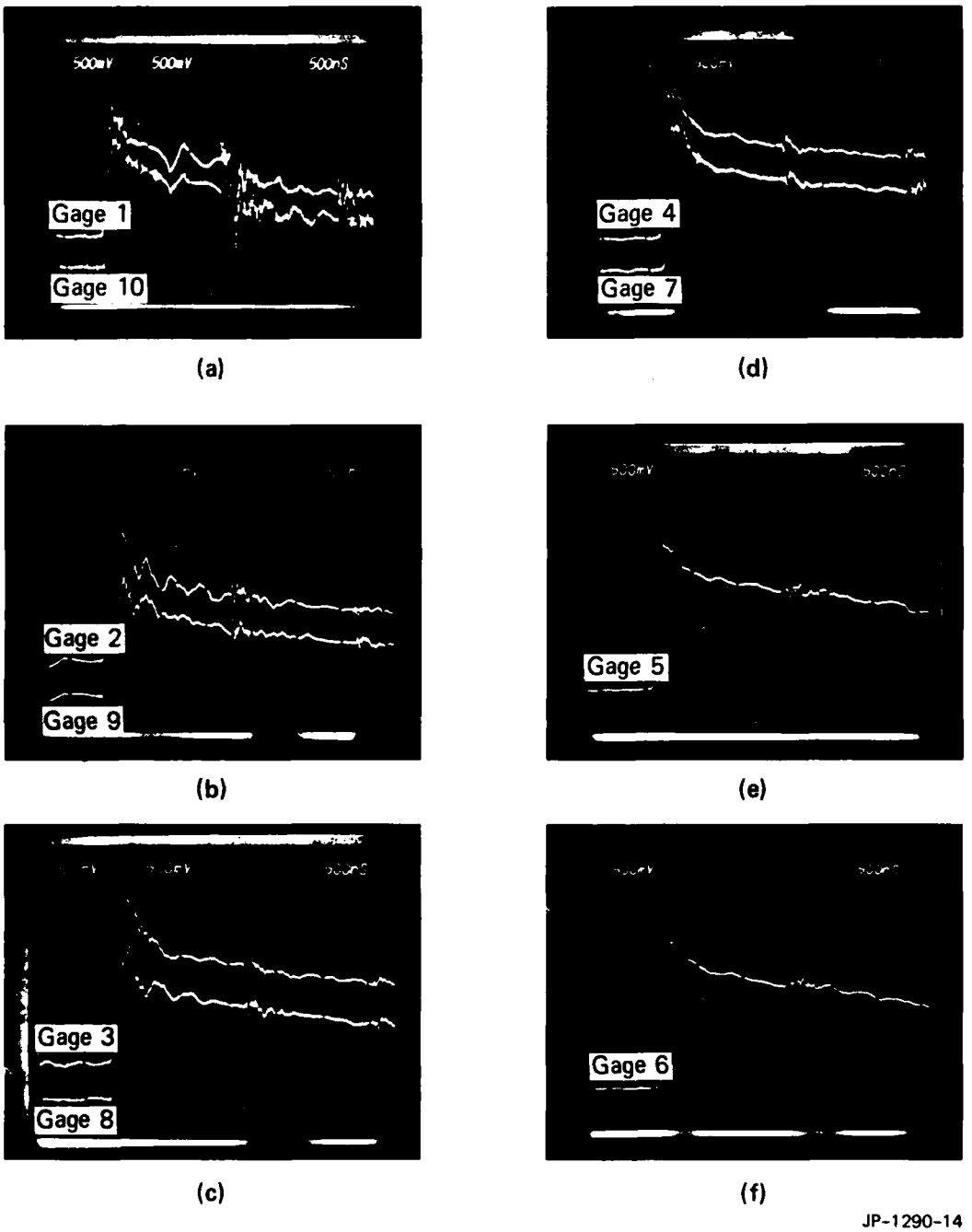

FIGURE 8 EPV GAGE RECORDS, COARSE-GRAINED AMATEX 20, SHOT 1290-2

depth in the target from the initiating plane. Because the cause is unknown and the oscillations do not interfere with data analysis except in the first two gage planes, the phenomenon was simply labeled noise and was not studied. Factors contributing to this noise may be the length of the gage leads (which may serve as antennas) and the conductivity of the explosive, especially in the reaction zone; the phenomenon is probably not caused by a real flow oscillation.

The second feature to note is the disturbance on a particular gage record when downstream gage enter the wave front. Again, we believe that these disturbances are electrical in origin and not the result of real flow oscillations. The disturbances are not large enough to interfere with data analysis, and they are useful for time-correlating the records. They may be caused by resistive coupling of gage circuits through the highly conductive wave front/reaction zone.

Lagrange Analysis

Procedure

Lagrange analysis based on particle velocity provides a quantitative description of the one-dimensional flow produced in a shock or detonation wave experiment from a set of particle velocity gage histories recorded along different particle paths. The flow variables are generated by integrating the equations of motion with flow derivatives estimated from the data supplied by the gage records. The momentum equation

$$\frac{\partial u}{\partial t}_h = -v_o \frac{\partial p}{\partial h}_t \tag{82}$$

where t and h denote time and Lagrange distance, and the subscript o denotes the unshocked conditon, gives dynamic Lagrange (p,u) relationships between pressure and particle velocity. The continuity equation

$$\frac{\partial v}{\partial t}_h = v_o \frac{\partial u}{\partial h}_t \tag{83}$$

gives dynamic Lagrange (v,u) relationships between specific volume and particle velocity. The elimination of v between these (p,u) and (v,u) relationships gives the corresponding Lagrange (p,v) relationships.

The voltage-time oscilloscope traces recorded by the particle velocity gages in detonating coarse-grained Amatex 20 (Figure 8) were the basis for the Lagrange analysis performed here. Before the experimental data can be used in a Lagrange analysis, the oscilloscope traces must be digitized and converted into particle velocity histories. The particle velocity histories were given the same numbers as the gages from which they were generated. It follows from Figure 7 that particle velocity histories were recorded by pairs of gages in each of five Lagrange planes in the sequence (1,10), (2,9), (3,8), (4,7), and (5,6). Selection and preparation of a single set of particle velocity histories for Lagrange analysis is discussed next.

Selection and Smoothing of Particle Velocity Records

First, the present particle velocity histories recorded in detonating Amatex 20 containing coarse-grained AN were compared with those recorded earlier[1] in detonating Amatex 20 containing baseline AN. The histories recorded in the coarse-grained Amatex 20 were found to be more noisy than those recorded in the baseline Amatex 20 as expected. The records produced by gage pairs (1,10) and (2,9) were considered to be too noisy for analysis and were discarded. The oscilloscope traces recorded by the pairs of gages (3,8), (4,7), and (5,6) were digitized and converted into particle velocity histories.

We first compared the particle velocity histories recorded by pairs of gages located in the same Lagrange plane. This comparison showed that the set of particle velocity histories exhibit the following characteristics:

- Histories 3 and 8 do not agree for approximately 0.5 μs at the wave front but are in good agreement over the last 3 μs.

- Histories 4 and 7 are noisy for ≈ 0.2 μs at the wave front but are in excellent agreement over ~ 4 μs.

- Histories 5 and 6 are in very good agreement over ~ 4 μs

We then compared the particle velocity histories (3, 4, 5,) from one side of the charge, then the corresponding particle velocity histories (8, 7, 6) from the other side of the charge, and finally all the particle velocity histories against each other.

The set (3,4,5) showed that

- Histories 3, 4, and 5 have respective peak particle velocities of ~ 2.2 mm/μs, ~ 2.3 mm/μs and 2.0 mm/μs at the wave front.

- Apart from exhibiting different peak structures, histories 4 and 5 agree for ~ 0.6 μs after the arrival of the wave front.

- The relative positions of histories 3, 4, and 5 over the last ~ 3.4 μs are compatible with the flow in a Taylor wave.

The set (8, 7, 6) showed that

- Histories 8, 7, and 6 have respective peak particle velocities of ~ 2.3 mm/μs, ~ 2.3 mm/μs, and 2.0 mm/μs.

- Apart from history 6 exhibiting a different peak structure than histories 8 and 7, the agreement among these histories for ~ 0.6 μs indicates the presence of a steady-state reaction zone in coarse-grained Amatex 20.

- The relative positions of histories 8, 7, and 6 over their last ~ 3.4 μs are compatible with the flow in a Taylor wave.

Comparison of all the particle velocity histories showed that

- Histories 4, 8, and 7 are in good agreement after the arrival of the wave front for ~ 0.6 μs as the particle velocity drops to ~ 1.6 mm μs, and except for a difference in peak structure the histories also agree with histories 5 and 6 over the same time interval.

  The relative positions of the records over their last ~ 3.4 μs are compatible with the flow in a Taylor wave.

We concluded that there are two distinct regions of flow behind the wave front in detonating coarse-grained Amatex 20: a steady-state reaction zone followed by an unsteady-state reaction zone.

We decided to use histories 4, 8, 7, and 6 to construct an idealized set of particle velocity histories for the Lagrange analysis. We first averaged the noise at the wave front on histories 4, 7, and 8 to make the particle velocity smooth and thereby standardize the shape of the reaction zone at the wave front. This smooth peak was then added to history 6 to generate a modified history 6 for the Lagrange analysis. Histories 8, 7, and the modified history 6 were then smoothed to obtain the idealized set of particle velocity histories for detonating coarse-grained Amatex 20 shown in Figure 9. The Lagrange analysis based on these particle velocity histories was performed with the GUINSY code[15] written by L. Seaman of SRI International.

Results

The results of this Lagrange analysis, i.e., the corresponding pressure-histories and the Lagrange compression and release paths in the (p-u) and (p-v) planes at the three gage locations, are shown in Figures 10, 11, and 12.

Discussion

The Detonation Process in Coarse-Grained Amatex 20

The fact that particle velocity histories recorded by different gages agree for a period of time after the arrival of the wave front was taken as evidence that the detonation wave in coarse-grained Amatex 20 is self-sustaining. Other properties of this self-sustaining detonation wave are obtained from the particle velocity histories and the results of the Lagrange analysis based on these histories.

Figures 11 and 12 show that the calculated loading and unloading paths at three Lagrange positions lie on a single curve. A particle of coarse-grained Amatex 20 entering the detonation wave is compressed along the Rayleigh line OR in the (p-u) and (p-v) planes and is then

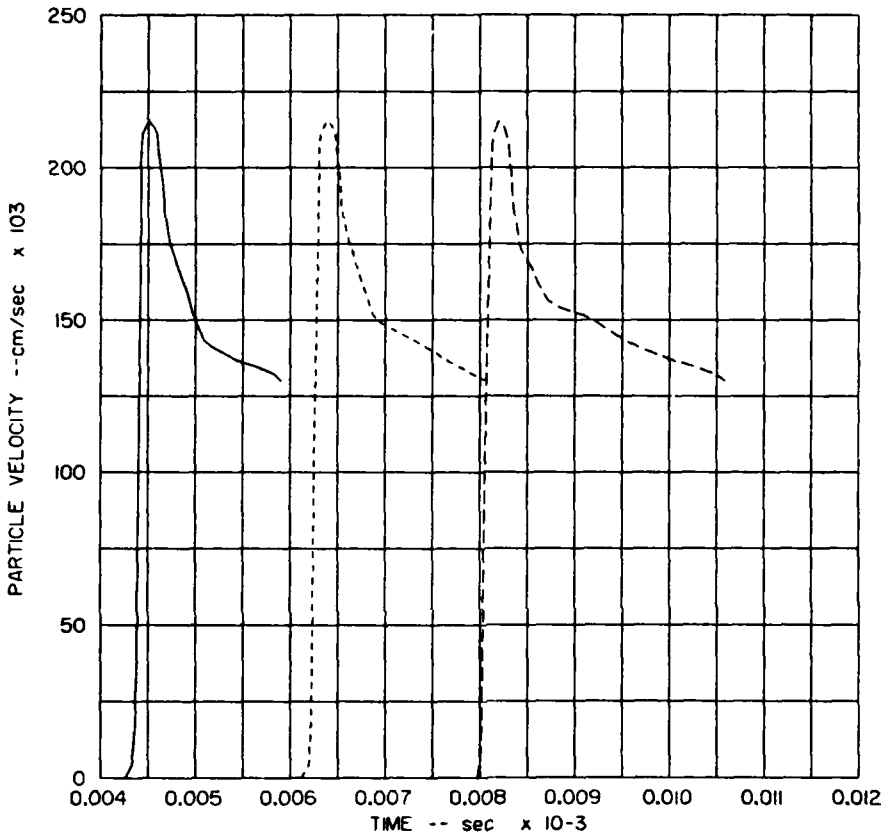

FIGURE 9 SMOOTHED PARTICLE VELOCITY HISTORIES IN DETONATING COARSE-GRAINED AMATEX 20, SHOT 1290-2

These idealized histories are based on the records from gages 8, 7, 6, and 4 and were used as input in the Lagrange analysis.

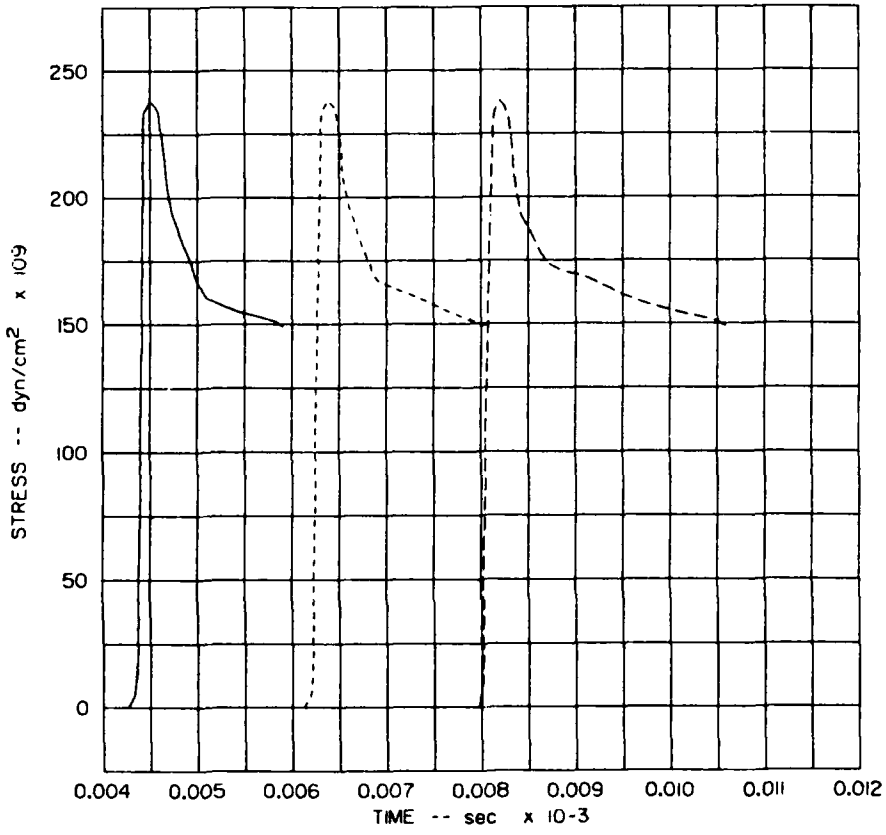

DATE = 26-MAR-82 SHOT 1290-2 AMATEX, PV8,7,6,SCS. 60,59,GAGES 1- 3

JA-1290-16

FIGURE 10 CALCULATED LAGRANGE PRESSURE HISTORIES AT THE GAGE POSITIONS IN DETONATING COARSE-GRAINED AMATEX 20

These results are based on the particle velocity histories shown in Figure 9.

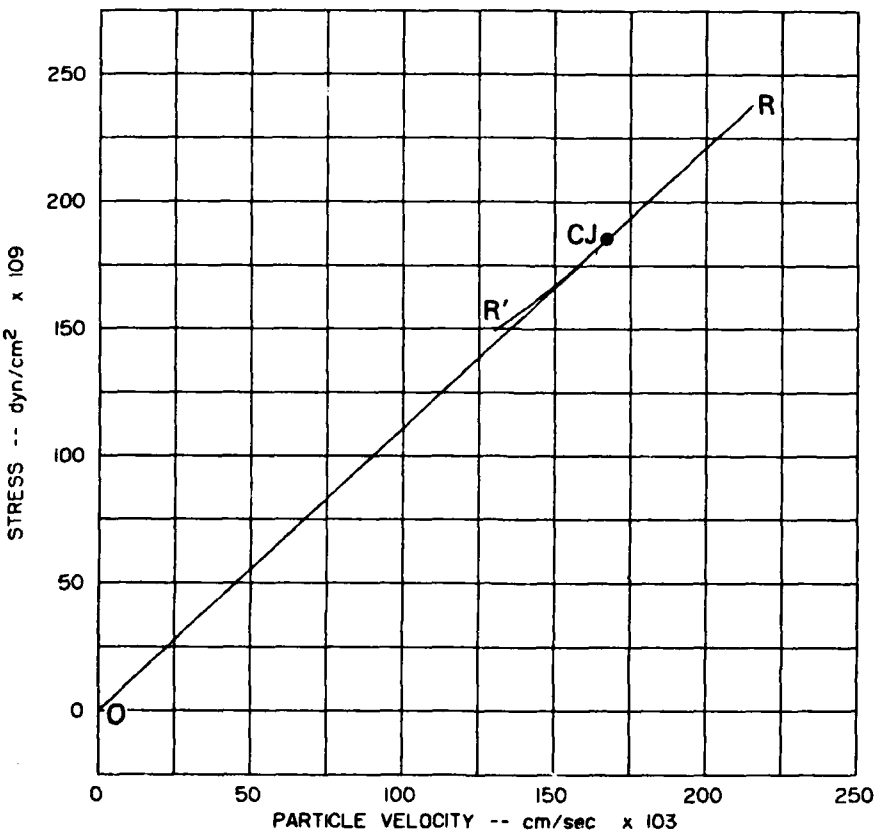

DATE = 26-MAR-82 SHOT 1290-2 AMATEX, PV8,7,6,SCS. 60,59,

JA-1290-17

FIGURE 11 CALCULATED LAGRANGE PRESSURE-PARTICLE VELOCITY SHOCK COMPRESSION AND ADIABATIC RELEASE PATHS AT THE GAGE POSITIONS IN DETONATING COARSE-GRAINED AMATEX 20

These results are based on the particle velocity histories shown in Figure 9.

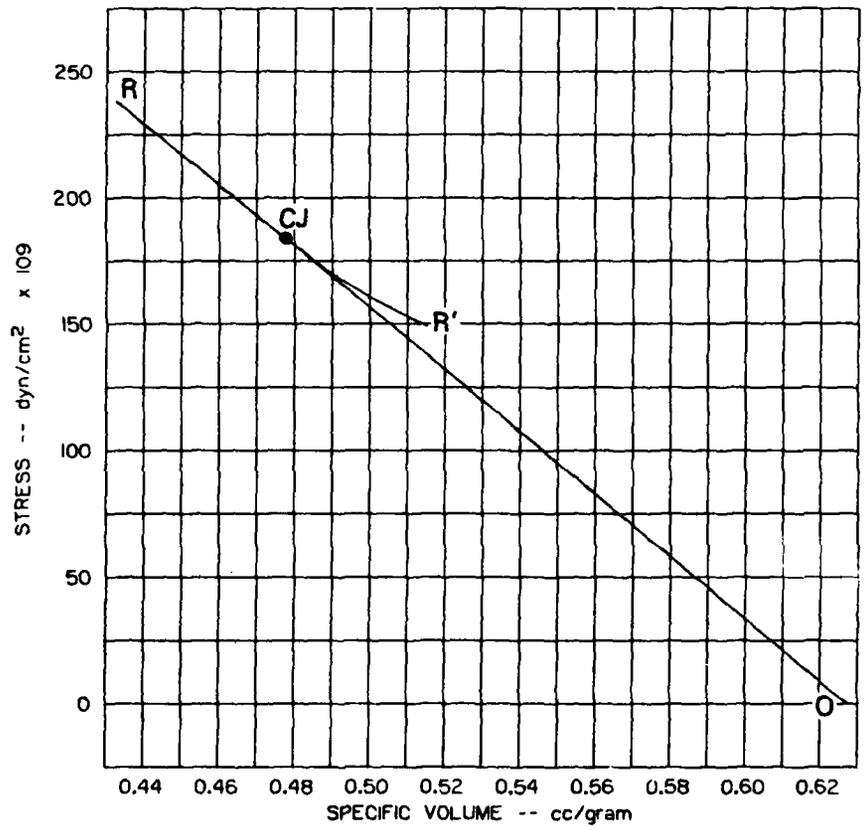

DATE = 26-MAR-82 SHOT 1290-2 AMATEX, PV8,7,6,SCS. 60,59,

JA-1290-18

FIGURE 12 CALCULATED LAGRANGE PRESSURE-SPECIFIC VOLUME SHOCK COMPRESSION AND ADIABATIC RELEASE PATHS AT THE GAGE POSITIONS IN DETONATING COARSE-GRAINED AMATEX 20

These results are based on the particle velocity histories shown in Figure 9.

rarified along the release adiabat RCJR'. RCJ coincides with the Rayleigh line and represents the steady-state reaction zone; CJR' diverges from the Rayleigh line and represents the unsteady zone. The unsteady zone is considered to be a Taylor wave because it is represented at different gage locations by a single curve in the (p-u) and (p-v) planes.

The particle velocity histories used to perform the Lagrange analysis and the resulting (p-u) and (p-v) paths were used to locate the CJ point at the end of the reaction zone. The resulting values of the CJ particle velocity and reaction time determined from the particle velocity records are u_{CJ} = 1.67 mm/μs and $\tau_{CJ} \sim 0.63$ μs. The values of D = 6.85 mm/μs and ρ_o = 1.594 g/cm^3 were then used with the Rankine-Hugoniot jump conditions to calculate the following values for the other CJ parameters: p_{CJ} = 182 kbar, v_{CJ} = 0.4742 cm^3/g, and K_{CJ} = 3.10.

The Role of AN in the Detonation Process in Amatex 20

To develop a better understanding of the role of AN in the detonation process in Amatex 20, we compared the present detonation parameters for Amatex 20 containing coarse-grained AN with those obtained earlier for Amatex 20 containing baseline AN. The earlier results were reexamined before making this comparison. This reexamination led us to conclude that the state previously identified as the CJ state has a higher particle velocity than the actual CJ state. Reassignment of the CJ particle velocity led to the following set of CJ parameters for baseline Amatex 20: D = 6.95 mm/μs, u_{CJ} = 1.94 mm/μs, p_{CJ} = 217 kbar, v_{CJ} = 0.4470 cm^3/g, K_{CJ} = 2.58, and $\tau_{CJ} \sim 0.5$ μs. The set of CJ parameters for coarse-grained Amatex 20 was as follows: D = 6.85 mm/μs, u_{CJ} = 1.67 mm/μs, p_{CJ} = 182 kbar, v_{CJ} = 0.4742 cm^3/g, K_{CJ} = 3.10, and $\tau_{CJ} \sim 0.63$ μs. Comparison of both sets clearly demonstrates that the particle size of AN influences the detonation process in Amatex 20.

The method of calculating detonation parameters developed by Kamlet[2-4] was modified and used to interpret the difference between these sets of CJ parameters. Kamlet's method is based on the results of

BKW detonation calculations and consequently assumes that an explosive is completely decomposed in the detonation process. Extension of this method to nonideal detonation[5] must therefore be based on the assumption that an explosive exhibits nonideal behavior because its detonation products do not attain chemical equilibrium. We thus assumed in treating Amatex 20 that the AN decomposes completely but that the reaction between the oxygen from the AN and the carbon from the RDX and TNT does not necessarily proceed to completion. This assumption is expressed in terms of the reaction coordinates introduced earlier in this report by the conditions $\lambda_1 = \lambda_2 = \lambda_3 = 1$ and $0 \leq \lambda_4 < 1$.

It is convenient to perform two limiting calculations, one with $\lambda_4 = 1$ corresponding to ideal detonation, and the other with $\lambda_4 = 0$ corresponding to nonideal detonation with complete decomposition of the explosive but no subsequent reaction among the detonation products. Values of experimentally determined detonation parameters smaller than those calculated with $\lambda_4 = 0$ can then be taken as strong evidence that the decomposition of AN is incomplete in the detonation process. This approach to nonideal detonation is considered to be more realistic than an approach based on TIGER or BKW calculations[9] because it is not restricted by the assumption of thermal equilibrium that such thermohydrodynamic codes use to make detonation calculations. Use of the thermal equilibrium condition and the chemical equilibrium conditions to calculate the composition of the detonation products in such codes automatically restricts their treatment of nonideality to incomplete decomposition of the explosive.[16]

Kamlet's semiempirical method for calculating detonation parameters of CHNO explosives with densities greater than 1.0 g/cm^3 uses the equations

$$P_{CJ} = \rho_o^2 K\phi \quad , \quad \phi = NM^{1/2} Q^{1/2} \quad , \quad K = 15.58 \tag{84}$$

$$D = A\phi^{1/2}(1 + B\rho_o) \quad , \quad A = 1.01 \quad , \quad B = 1.30 \tag{85}$$

where N is the number of moles of gaseous detonation products per gram of explosive, M is the average molecular weight of these gases, Q is the standard heat of reaction per gram, and ρ_o is the initial density. Values of N, M, and Q are estimated from an abitrary assumption about the detonation product's composition, so that calculations require no other input than the explosive's elemental composition, loading density, and heat of formation. The H_2O-CO_2 arbitrary assumption about the detonation products composition and the heats of formation for RDX, TNT, AN, and Amatex 20 shown in Table 5 were used to calculate the values of N, M, and ϕ shown in Table 5. The values of a, b, c, and d for 100 gm of Amatex 20 considered as a composite explosive are a = 1.5037, b = 3.4216, c = 2.0692, and d = 3.0978.

We use the superscript e to denote that the detonation products attain chemical equilibrium, and we use the superscript f to denote that the composition of the detonation products is frozen with the products from each component in chemical equilibrium. To make the ideal detonation calculations for Amatex 20 ($\lambda_4 = 1$), we set $\phi = \phi^e_{20} = 6.070$ and use Eqs. (84) and (85) to calculate the CJ pressures and detonation velocities for $\rho_o = 1.613$ g/cm^3 and $\rho_o = 1.594$ g/cm^3. To make the limiting nonideal detonation calculation for Amatex 20 ($\lambda_4 = 0$), we assume that each explosive component decomposes into its own equilibrium detonation products, set $\phi = \phi^f_{20} = 0.2\ Q^e_{RDX} + 0.4\ Q^e_{TNT} + 0.4\ Q^e_{AN} = 4.865$, and use Eqs. (84) and (85) to calculate the CJ pressures and detonation velocities for $\rho_o = 1.613$ g/cm^3 and $\rho_o = 1.594$ g/cm^3. The results of these calculations are shown in Table 6.

Experimental and calculated values of CJ parameters for Amatex 20 can now be compared to investigate the role of AN in the detonation process. The relationship between the experiment CJ parameters for baseline Amatex 20, $\{D = 6.95$ mm/μs, $p_{CJ} = 217$ kbar, $u_{CJ} = 1.9$ mm/μs$\}$, and those calculated for the same initial density, $D = 6.90$ mm/μs, $p_{CJ} = 197$ kbar, $u_{CJ} = 1.77$ mm/ μs, $\lambda_4 = 0$, is consistent with the following conclusions:

Table 5

VALUES OF DETONATION PARAMETERS FOR RDX, TNT, AN, AND AMATEX 20

Explosive	ΔH_f^o (kcal/100g)	N (moles/g)	M (g/mole)	(ϕ)
RDX, $C_3H_6N_6O_6$	6.62	0.0338	27.20	6.783
TNT, $C_7H_5N_3O_6$	-7.84	0.0253	28.52	4.838
AN, $H_4N_2O_3$	-109.12	0.0437	22.87	3.932
Amatex 20, $C_aH_bN_cO_d$	-45.5	0.344	26.25	6.070

Table 6

CALCULATED CJ PARAMETERS FOR AMATEX 20

Amatex 20	ρ_o (g/cm^3)	P_{CJ} (kbar)	D (mm/μs)	u_{CJ} (mm/μs)	K_{CJ}
$\lambda_4 = 1$, $\phi_{20}^e = 6.070$	1.613	246	7.71	1.98	2.89
$\lambda_4 = 0$, $\phi_{20}^f = 4.865$	1.613	197	6.90	1.77	2.89
$\lambda_4 = 1$, $\phi_{20}^e = 6.070$	1.594	240	7.64	1.97	2.88
$\lambda_4 = 0$, $\phi_{20}^f = 4.865$	1.594	192	6.85	1.76	2.88

(1) In the planar detonation process in baseline Amatex 20, AN with a mean particle size of ~0.7 mm decomposes completely in the reaction zone, but the detonation products produced by RDX, TNT, and AN do not attain chemical equilibrium.

(2) In the reaction zone of the planar detonation wave in baseline Amatex 20, the rate of decomposition of AN is faster than the rate of recombination of the oxygen produced by the AN and the carbon produced by RDX and TNT.

Comparison of the experimental CJ parameters for coarse-grained Amatex 20, $\{D = 6.85$ mm/μs, $p_{CJ} = 182$ kbar, $u_{CJ} = 1.67$ mm/μs$\}$, with those calculated for the same initial density, $\{D = 7.64$ mm/μs, $p_{CJ} = 240$ kbar, $u_{CJ} = 1.97$ mm/ μs, $\lambda_4 = 1\}$, and $\{D = 6.85$ mm/μs, $p_{CJ} = 192$ kbar, $u_{CJ} = 1.76$ mm/ μs, $\lambda_4 = 0\}$ does not lead directly to a conclusion because the experimental values are approximately equal to those calculated for no reaction among the detonation products.

A conclusion can be reached, however, by assuming that the reaction processes in coarse-grained Amatex 20 are similar to those in baseline Amatex 20 and taking account of the following facts:

- In baseline Amatex 20, the recombination reaction between oxygen and carbon proceeds in the reaction zone as the AN decomposes.
- The reaction time in coarse-grained Amatex 20 is longer than the reaction time in baseline Amatex 20.
- The experimentally determined value of $K_{CJ} = 3.10$ for coarse-grained Amatex 20 is larger than the values of K_{CJ} resulting from the detonation calculations.

It follows from our assumption about the reaction processes in Amatex 20 that the recombination reaction between oxygen and carbon proceeds in the reaction zone of coarse-grained Amatex 20 for a longer time than it proceeds in the reaction zone of baseline Amatex 20. Because this recombination reaction liberates more energy than the decomposition of AN, we propose the following conclusion, compatible with our first and second conclusions:

(3) In the planar detonation process in coarse-grained Amatex 20, AN with a mean particle use of ~2 mm does not decompose completely in the reaction zone, and the detonation products produced by RDX, TNT, and AN do not attain chemical equilibrium.

The higher value of K_{CJ} also supports the conclusion that the decomposition of AN is incomplete in the reaction zone in coarse-grained Amatex 20.

Calculations with the burning rate of AN written as a function of pressure using the reaction times for baseline and coarse-grained Amatex 20 are recommended to estimate the amount of unreacted AN in the reaction zone of coarse-grained Amatex 20.

REFERENCES

1. M. Cowperthwaite and J. T. Rosenberg, "Lagrange Gage Studies of Nonideal Explosives Containing NH_4NO_3," Final Report prepared for U.S. Army Research Office, Contract DAAG29-76-C-0033, SRI International, Menlo Park, California (October 1979).

2. M. J. Kamlet and S. J. Jacobs, "Chemistry of Detonations. I: A Simple Method for Calculation Detonation Properties of C-H-N-O Explosives," J. Chem. Phys., 48, 23 (1968).

3. M. J. Kamlet and J. E. Ablard, "Chemistry of Detonations. II: Buffered Equilibria," J. Chem. Phys., 48, 36 (1968).

4. M. J. Kamlet and C. Dickinson, "Chemistry of Detonations. III: Evaluation of the Simplified Calculational Method for Chapman-Jouguet Detonation Pressures on the Basis of Available Experimental Information," J. Chem. Phys., 48, 43 (1968).

5. Private communications with Dr. J. M. Short and Dr. M. J. Kamlet of Naval Surface Weapons Center, White Oak, Silver Spring, Maryland (1983).

6. Ya. B. Zeldovich, "On the Theory of the Propagation of Detonation in Gaseous Systems," Sov. Phys. IETP, 10, 542 (1940).

7. J. von Neumann, "Theory of Detonation Waves," OSRD 549 (1942).

8. W. Doering, "On Detonation Processes in Gases," Ann Physik, 43, 421 (1943).

9. W. Fickett and W. C. Davis, Detonation (University of California Press, Berkeley, Los Angeles, and London, 1979, pp. 16-18.

10. M. Cowperthwaite, "A Constitutive Model for Calculating Chemical Energy Release Rates from the Flow Fields in Shocked Explosives," in Seventh Symposium (International) on Detonation, J. M. Short, Ed., NSWC MP 82-334 (Naval Surface Weapons Center, White Oak, Silver Spring, Maryland) p. 498.

11. M. Cowperthwaite and J. T. Rosenberg, "A Multiple Lagrange Gage Study of the Shock Initiation Process in Cast TNT," in Proceedings of the Sixth Symposium (International) on Detonation, D. J. Edward, Ed., ACR-221 (Office of Naval Research, Department of the Navy, 1981, p. 786.

12. M. Cowperthwaite and J. T. Rosenberg, "Lagrange Gage Studies in Ideal and Nonideal Explosives," in Seventh Symposium (International) on Detonation, J. M. Short, Ed., NSWC MP 82-334, (Naval Surface Weapons Center, White Oak, Silver Spring, Maryland) p. 1072.

13. V. M. Zaitzev, P. F. Pokhil, and K. K. Shvedov, "The Electromagnetic Method for the Measurement of Velocities of Detonation Products," Doklady Acad. Sci. USSR, 132(6), 1339 (1960).

14. S. J. Jacobs and David J. Edwards, "Experimental Study of the Electromagnetic Velocity Gage Technique," in Proceedings of Fifth Symposium (International) on Detonation, ACR-184 (Office of Naval Research, Department of the Navy, 1970, p. 413.

15. L. Seaman, "Lagrangian Analysis for Multiple Stress and Velocity Gages in Attenuating Waves," J. Appl. Phys., 45, 4303 (1974).

16. J. N. Johnson, C. L. Mader, and S. Goldstein, "Performance Properties of Commercial Explosives," Propellants, Explosives, Pyrotechnics, 8, 8 (1983).